Pharmacological Research 142 (2019) 151–168

Contents lists available at ScienceDirect

Pharmacological Research

journal homepage: www.elsevier.com/locate/yphrs

Invited Review

Targeting ERK1/2 protein-serine/threonine kinases in human cancers

Robert Roskoski Jr.

Blue Ridge Institute for Medical Research, 3754 Brevard Road, Suite 116, Box 19, Horse Shoe, NC, 28742-8814, United States

ARTICLE INFO

Chemical compounds studied in this article:
Binimetinib (PubMED CID: 10288191)
CC-90003 (PubMED CID: 9033117)
Encorafenib (PubMED CID: 50922675)
KO-947 (PubMED CID: 91668256)
LY3214996 (PubMED CID: 121408882)
MK-8353 (PubMED CID: 58282870)
Ravoxertinib (PubMED CID: 71727581)
Ulixertinib (PubMED CID: 11719003)
SCH772984 (PubMED CID: 24866313)
Vemurafenib (PubMED CID: 42611257)

Keywords:
Catalytic spine
K/E/D/D
Protein kinase inhibitor classification
Protein kinase structure
Regulatory spine
MAP kinase pathway

ABSTRACT

ERK1 and ERK2 are key protein kinases that contribute to the Ras-Raf-MEK-ERK MAP kinase signalling module. This pathway participates in the control of numerous processes including apoptosis, cell proliferation, the immune response, nervous system function, and RNA synthesis and processing. MEK1/2 activate human ERK1/2 by first catalyzing the phosphorylation of Y204/187 and then T202/185, both residues of which occur within the activation segment. The phosphorylation of both residues is required for enzyme activation. The only Raf substrates are MEK1/2 and the only MEK1/2 substrates are ERK1/2. In contrast, ERK1/2 catalyze the phosphorylation of many cytoplasmic and nuclear substrates including transcription factors and regulatory molecules. The linear MAP kinase pathway branches extensively at the ERK1/2 node. ERK1/2 are proline-directed kinases that preferentially catalyze the phosphorylation of substrates containing a PxS/TP sequence. The dephosphorylation and inactivation of ERK1/2 is catalyzed by dual specificity phosphatases, protein-tyrosine specific phosphatases, and protein-serine/threonine phosphatases. The combined functions of kinases and phosphatases make the overall process reversible. To provide an idea of the complexities involved in these reactions, somatic cell cycle progression involves the strict timing of more than 32,000 phosphorylation and dephosphorylation events as determined by mass spectrometry. The MAP kinase cascade is perhaps the most important oncogenic driver of human cancers and the blockade of this signalling module by targeted inhibitors is an important anti-tumor strategy. Although numerous cancers are driven by MAP kinase pathway activation, thus far the only orally effective approved drugs that target this signaling module are used for the treatment of *BRAF*-mutant melanomas. The best treatments include the combination of B-Raf and MEK inhibitors (dabrafenib and trametinib, encorafenib and binimetinib, vemurafenib and cobimetanib). However, resistance to these antagonists occurs within one year and additional treatment options are necessary. Owing to the large variety of malignancies that are driven by dysregulation of the MAP kinase pathway, additional tumor types should be amenable to MAP kinase pathway inhibitor therapy. In addition to new B-Raf and MEK inhibitors, the addition of ERK inhibitors should prove helpful. Ulixertinib, MK-8353, and GDC-0994 are orally effective, potent, and specific inhibitors of ERK1/2 that are in early clinical trials for the treatment of various advanced/metastatic solid tumors. These agents are effective against cell lines that are resistant to B-Raf and MEK1/2 inhibitor therapy. Although MK-8353 does not directly inhibit MEK1/2, it decreases the phosphorylation of ERK1/2 as well as the phosphorylation of RSK, an ERK1/2 substrate. The decrease in RSK phosphorylation appears to be a result of ERK inhibition and the decrease in ERK1/2 phosphorylation is related to the inability of MEK to catalyze the phosphorylation of the ERK–MK-8353 complex; these decreases characterize the ERK dual mechanism inhibition paradigm. Additional work will be required to determine whether ERK inhibitors will be successful in the clinic and are able to forestall the development of drug resistance of the MAP kinase pathway.

1. The Ras-Raf-MEK-ERK (MAP kinase) signaling pathway

Protein kinases play pivotal regulatory roles in nearly every aspect of cell biology [1–3]. They control cell growth, cell proliferation, cell survival, differentiation, the immune response, metabolism, nervous system function, and transcription. Because protein phosphorylation

Abbreviations: AS, activation segment; C-spine, catalytic spine; CDK, cyclin-dependent kinase; CS1, catalytic spine residue 1; CL, catalytic loop; DUSP, dual specificity phosphatase; EGFR, epidermal growth factor receptor; GAP, GTPase activating protein; GEF, guanine nucleotide exchange factor; GK, gatekeeper; GRL, glycine-rich loop; KID, kinase insert domain; LE, ligand efficiency; LipE, lipophilic efficiency; NSCLC, non-small cell lung cancer; PDGFR, platelet-derived growth factor receptor; PKA, protein kinase A; pERK, phosphorylated ERK; R-spine, regulatory spine; RS1, regulatory spine residue 1; Sh2, shell residue 2; VEGFR, vascular endothelial growth factor receptor

E-mail address: rrj@brimr.org.

https://doi.org/10.1016/j.phrs.2019.01.039
Received 16 January 2019; Accepted 18 January 2019
Available online 20 February 2019

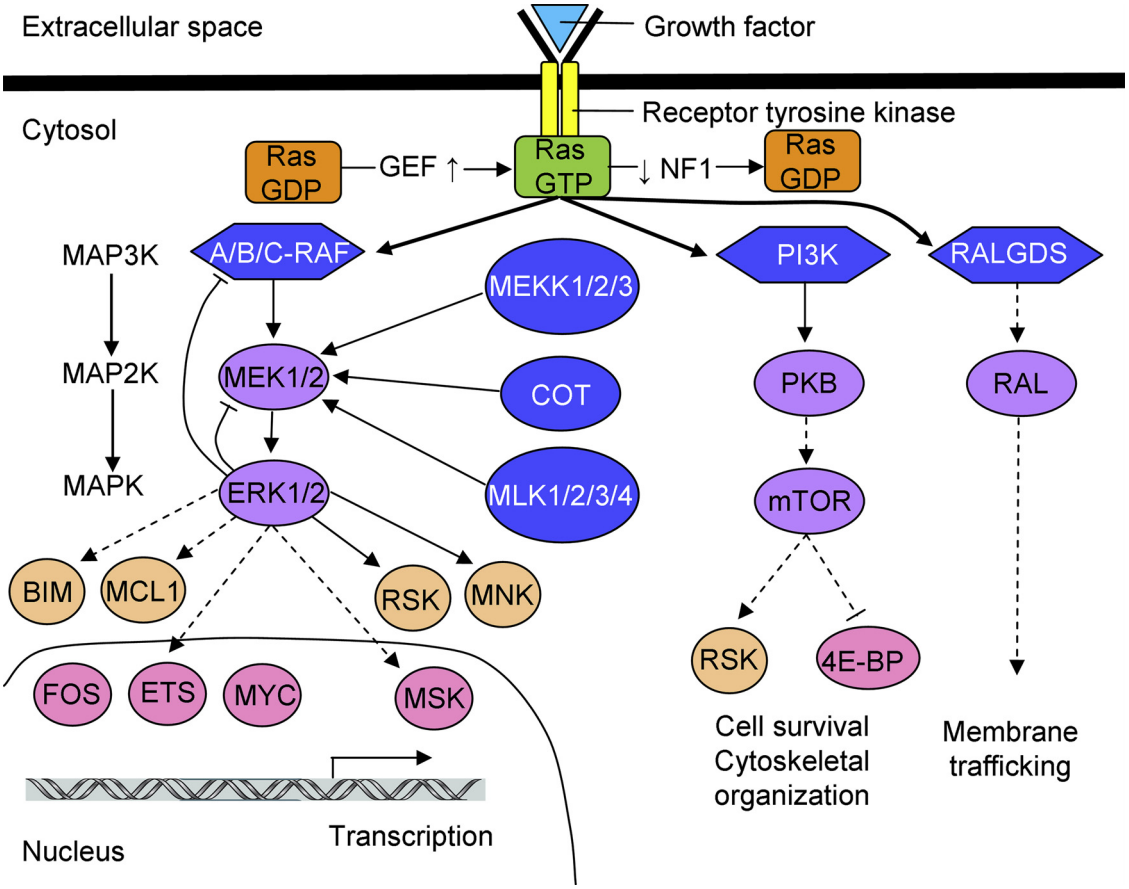

Fig. 1. Ras-GTP effector modules including the evolutionarily conserved Ras-Raf-MEK-ERK MAP kinase pathway. GEF action increases the level of Ras-GTP and NF1 activity decreases the level of Ras-GTP. The dashed lines indicate that several steps may be involved. GEF, guanine nucleotide exchange factor; NF1, neurofibromin-1. Adapted from Ref. [12] with copyright permission from Elsevier.

involves the action of both protein kinases as well as phosphoprotein phosphatases, phosphorylation-dephosphorylation is an overall reversible process. To provide an idea of the complexities involved in these reactions, somatic cell cycle progression involves the precise timing of more than 32,000 phosphorylation and dephosphorylation reactions as determined by mass spectrometry [4]. Moreover, the dysregulation of protein kinase signaling occurs in many diseases including cardiovascular, inflammatory, and neurodegenerative disorders as well as cancers. Owing to the importance of the overactivity of protein kinases in the pathogenesis of a variety of common diseases, it is estimated that about of 20–33% of all drug discovery programs target protein kinases. These enzymes catalyze the following reaction:

$$MgATP^{1-} + \text{protein–O:H} \rightarrow \text{protein–O:}PO_3^{2-} + MgADP + H^+$$

Based upon the identity of the substrate, these enzymes are classified as protein-tyrosine or protein-serine/threonine kinases [5]. Enzymes such as MEK1/2, which catalyze the phosphorylation of tyrosine and then threonine in the activation segment of ERK1/2, make up a small group of so-called dual-specificity protein kinases [6,7]. These dual-specificity enzymes are evolutionarily classified as protein-serine/threonine kinases.

The MAP kinase signalling module is perhaps the most important oncogenic driver of human malignancies [8–12]. This evolutionarily conserved pathway relays extracellular signals to intracellular signaling cascades. The MAP kinase pathway is activated by a variety of transmembrane receptors. For example, the activated epidermal growth factor receptor (EGFR) becomes auto-phosphorylated at tyrosine residues that interact with guanine nucleotide exchange factors (GEFs) such as SOS (from *Drosophila* son of sevenless) as well as other adaptor proteins. The GEFs facilitate the conversion of dormant Ras-GDP to the functional Ras-GTP in the plasma membrane [13–15]. It is important to note that generally all of Ras biochemistry and signaling occur within the inner leaflet of the plasma membrane. The *RAS* (Rat sarcoma) gene family includes three members: *HRAS*, *KRAS*, and *NRAS*. These Ras proteins toggle between inactive and active forms; the conversion of dormant Ras-GDP to active Ras-GTP turns the switch on and the intrinsic Ras-GTPase activity promoted by the GTPase activating proteins (GAPs) such as NF1 (neurofibromin-1) turns the switch off.

The molecular weight of each of the three Ras proteins is about 21 kDa. In contrast, the molecular weights of the multidomain GEFs and GAPs are large (150–300 kDa) thereby permitting an astonishing variety of interactions with lipids, proteins, and regulatory molecules that control the levels of dormant and active Ras [15]. To activate downstream members of the MAP kinase module, Ras-GTP stimulates the formation of active homodimers or heterodimers made up of A-Raf, B-Raf, and C-Raf by an intricate process (the Raf acronym corresponds to *R*apidly *a*ccelerated *f*ibrosarcoma, first described in mice). The Raf enzymes are protein-serine/threonine protein kinases that catalyze the phosphorylation and activation of MEK1 and MEK2 where MEK corresponds to *M*AP/*E*RK *K*inase. The MEK proteins, in turn, catalyze the phosphorylation and activation of ERK1 and ERK2 (*E*xtracellular Signal-*R*egulated protein *K*inases).

The A/B/C-Raf enzymes and MEK1/2 have very narrow substrate specificity [15–19]. Accordingly, the only known Raf substrates are MEK1/2 and the only known MEK1/2 substrates are ERK1/2. To further exemplify their narrow substrate specificity, MEK1/2 are unable to catalyze the phosphorylation of denatured ERK1/2 and they are unable to catalyze the phosphorylation of peptides with the sequence

corresponding to the activation segment of ERK1/2, the physiological substrate. In contrast to the Raf and MEK enzymes, ERK1/2 have wide substrate specificity that allows them to catalyze the phosphorylation of hundreds of different cytosolic and nuclear proteins [19,20]. The linear MAP kinase pathway branches extensively at the ERK1/2 node. The Kinase Suppressors of Ras (KSR1/2) are the closest relatives of the Raf family kinases (www.kinase.com/human/kinome). KSR1/2 are impaired protein kinases (but not kinase dead) that are able to function as scaffolds that assemble Raf, MEK, and ERK to increase signaling efficiency [21]. The outcome of KSR1/2 function is context-dependent and varies with the concentration of the various members of the MAP kinase pathway; as a result, these proteins can be stimulatory or inhibitory.

The MAP kinase module consists of a hierarchical tier of three protein kinases: (i) MAP3K (MAPK kinase kinase), (ii) MAP2K (MAPK kinase), and (iii) and MAPK. Although A/B/C-Raf are near the proximal end of the MAP kinase cascade, MEKK1/2/3, COT (also known as *C*ancer *O*saka *T*hyroid kinase or MAP3K8), and MLK1/2/3/4 are other ERK1/2 MAP3Ks that participate in cell type and stimulation specific responses (Fig. 1). Ras-GTP has additional downstream effector pathways including the phosphatidylinositol 3-kinase (PI3 kinase) and RalGDS modules [22–24]. PKB/Akt is downstream from PI3 kinase. The MAP kinase pathway contains short-term negative feedback servomechanism loops that include the phosphorylation of Raf enzymes as well as MEK1/2 as catalyzed by ERK1/2. Long-term feedback results from the synthesis of DUSP5/6 (dual specificity phosphatases-5/6) that catalyze the dephosphorylation and inactivation of ERK1/2 within the nucleus and cytoplasm [25]; activation of ERK1/2 thus dampens the stimulatory response. The existence of parallel downstream pathways suggests a strategy of combining targeted inhibitors of Raf, MEK, or ERK of the MAP kinase pathway along with inhibition of PI3 kinase or PKB/Akt in the treatment of various neoplasms [26].

2. Treatment of human malignancies with Raf and MEK inhibitors

RAS mutations occur in about 33% of all cancers [27,28]. *KRAS* mutations occur in about 70% of pancreatic ductal adenocarcinomas, 40% of colorectal cancers, 35% of non-small cell lung cancers (NSCLC), 20% of papillary thyroid cancers, 10% of breast and ovarian cancers, and 10% of acute myelogenous and acute lymphoblastic leukemias. Additionally, *NRAS* mutations occur in about 20% of melanomas and 15% of anaplastic thyroid cancers and follicular thyroid cancers; mutations of *HRAS* occur in about 20% of urothelial bladder carcinomas and 2% of renal cell carcinomas. Although investigators have attempted to develop Ras inhibitors for decades, only recently has there been a modicum of success [29–34]. This is related to the lack of a reasonably sized Ras drug-binding pocket. However, no direct Ras inhibitors have yet entered clinical trials. Alternatively, combinations of Raf and MEK inhibitors that target the MAP kinase pathway have been developed. Thus far, these inhibitors have been approved for the treatment of advanced melanomas with activating mutations in *BRAF*; the term advanced in the oncology setting usually means unresectable, metastatic, or both. Owing to the large variety of malignancies that are driven by the MAP kinase pathway, one anticipates that Raf and MEK inhibitors will be used to treat additional cancers.

There is considerable interest in developing ERK1/2 inhibitors as therapeutic agents. Because Raf and MEK inhibitors are effective and the MAP kinase pathway is linear (Ras-Raf-MEK-ERK), ERK represents a logical and valid target. Inhibiting the terminal kinase of the MAP kinase pathway represents a promising strategy for the treatment of a broad spectrum of malignancies that harbor pathway-activating machinery. Moreover, resistance to Raf and MEK inhibitors is very often the result of reactivation of this signaling module so that ERK represents another target that may forestall acquired resistance to such antagonists as well as producing a primary therapeutic response. The discovery of clinically effective ERK1/2 inhibitors has lagged far behind the development Raf and MEK inhibitors despite being druggable entities.

The estimated number of new cases of skin melanomas in the United States in 2018 was 91,000 and the estimated number of deaths was 9300 (https://seer.cancer.gov/statfacts/html/melan.html). It is one of the more common malignancies ranking below lung, breast, prostate, and colorectal cancers. At the time of diagnosis, about 84% have localized disease, 9% have spread to regional lymph nodes, 4% have distant metastasis, and 4% are unstaged. The overall five-year survival is about 92%. This malignancy is most frequently diagnosed among people aged 65–74 and is more common in men than women (ratio 3:2). It occurs in individuals of fair complexion and those who have been exposed to sunlight over long periods of time. The incidence in Caucasians is about ten-fold greater than any other racial/ethnic group. The rates for new melanoma of the skin cases have been rising 1.5% over the last ten years, but the death rates have been falling 1.2% each year from 2006–2015.

Mutational oncogenic activation of the Ras-Raf-MEK-ERK pathway occurs in a wide variety of cancers including more than 90% of skin melanomas [35,36]. The Cancer Network consortium studied the genetic background of skin melanomas in 331 patients based upon DNA, RNA, and protein analysis [36]. They reported that the occurrence of *BRAF* mutations was 52%, that of *NRAS* mutations was 28%, and that of *NF1* mutations was 14%; they classified the remainder of cases as triple-WT (wild type). Both the gain-of-function *BRAF* and *NRAS* mutations and the loss-of-function *NF1* mutations result in the activation of the MAP kinase pathway. *BRAF* mutations occur in 10–70% of thyroid cancers (depending upon the histology), about 10% of colorectal cancers, and 3–5% of NSCLC cases [37–40].

The observation that activating *BRAF* mutations occur in the majority of melanomas [41] provided the rationale for the development of B-Raf inhibitors [42]. Sorafenib was initially developed as a C-Raf protein kinase inhibitor (reflected in its name so*rafenib*). However, this drug is a VEGFR1/2/3, Kit, PDGFR, RET, and Flt3 multikinase inhibitor. Several clinical trials examined the efficacy of sorafenib in patients with metastatic melanomas, but the results were not encouraging. For example, sorafenib produced a favorable clinical response in fewer than 5% of patients with melanomas [43]. Its activity against $BRAF^{V600E}$ mutants and the wild type enzymes was less than its activity against C-Raf, which explains in part its lack of effectiveness in the treatment of these patients. Sorafenib is currently FDA-approved for the treatment of renal cell, differentiated thyroid, and liver carcinomas. In another clinical trial, Chapman et al. compared vemurafenib with dacarbazine (a DNA-alkylating agent) in 675 randomized melanoma patients carrying the $BRAF^{V600E}$ mutation [44]. They reported that the overall response rate for vemurafenib was 48% compared with that for dacarbazine of 5%. Adverse effects of vemurafenib included nausea, diarrhea, fatigue, joint pain (arthralgia), and skin rashes along with the formation of (i) well-differentiated squamous cell skin carcinomas or (ii) keratoacanthomas. Such tumors can be readily identified by inspection and are easy to excise. Nevertheless, the formation of these tumors is clearly an undesired result. Diarrhea, fatigue, and skin rashes are adverse incidents that are associated with the treatment of many protein kinase inhibitors [45]. Vemurafenib was approved by the FDA for the treatment of $BRAF^{V600E}$ melanomas in 2011.

Dabrafenib was the second small molecule B-Raf inhibitor that entered clinical trials in comparison with cytotoxic dacarbazine. Hauschild et al. reported that the response rate for dabrafenib was about 50% compared with that for dacarbazine of about 6% [46]. The dabrafenib progression-free survival was 5.1 months while that for dacarbazine was 2.7 months. The adverse events produced by dabrafenib were comparable to those produced by vemurafenib. However, vemurafenib is associated with a photosensitivity response [44] while dabrafenib is likely to produce fever [46]. Dabrafenib was approved by the FDA for the treatment of patients with advanced melanomas with the $BRAF^{V660E}$ mutation in 2013 (www.brimr.org/PKI/PKIs.htm). As was the case for vemurafenib, about 20% of patients receiving dabrafenib develop keratoacanthomas. The keratoacanthomas are treated by

surgical excision and these drugs can be continued without any dose adjustment. However, each of these drugs is ineffective in the treatment of patients who lack the $BRAF^{V600E}$ mutation.

Dabrafenib and vemurafenib each produce the paradoxical activation of the MAP kinase pathway in wild type *BRAF* cells [12,16,19]. It is contradictory in the sense that a B-Raf antagonist, which is one component of the module, results in the overall activation of the pathway. Such paradoxical activation leads to drug-induced skin lesions (keratoacanthomas) as noted above. Owing to paradoxical activation, both dabrafenib and vemurafenib promote growth and metastasis of tumor cells bearing *RAS* mutations in animal studies and they are contraindicated for the treatment of cancer patients with wild type *BRAF*, including patients with activating *RAS* mutations. The precise mechanism of MAP kinase pathway activation is unclear despite extensive experimentation, but drug-induced Raf dimerization appears to be an essential component of this process. See Refs. [16,19] for a discussion of the possible mechanisms that result in this paradoxical response to B-Raf inhibitors.

Although nearly all patients with melanomas with the $BRAF^{V600E}$ mutation derive clinical benefit, median progression-free survival is only six months and more than 90% of patients develop resistance within one year [45]. This rapid incidence of secondary resistance prompted the study of other MAP kinase pathway inhibitors. One of first of these alternative inhibitors was trametinib, which is a potent antagonist of MEK1/2. In a clinical trial with 322 melanoma patients possessing $BRAF^{V600E/K}$ mutations, Flaherty et al. reported that trametinib produced an improved overall response rate (22% vs. 8%) and progression-free survival (4.8 vs. 1.5 months) when compared with groups receiving cytotoxic dacarbazine or paclitaxel [47]. Peripheral edema, diarrhea, and skin rashes were the principal trametinib adverse events, which were easily managed. Mild grade 1 or 2 ocular toxicity (blurred vision) was reported in 9% of the patients most likely resulting from serous retinopathy, a reversible disorder. In contrast to dabrafenib or vemurafenib, the trametinib patients failed to develop secondary skin neoplasms.

In a clinical trial with 97 patients, Kim et al. reported that trametinib had significant clinical activity in B-Raf-inhibitor–naive patients who were previously treated with chemotherapy, immunotherapy, or both [48]. Conversely, they found that trametinib had minimal activity as a second-line treatment in patients who were previously treated with a B-Raf inhibitor. Consequently, these authors suggested that B-Raf-inhibitor resistance mechanisms also confer resistance to MEK-inhibitor monotherapy. Accordingly, the FDA approved trametinib initially (2013) as a monotherapy for patients who had not received B-Raf inhibitor therapy (www.brimr.org/PKI/PKIs.htm).

In a clinical trial involving 247 patients with advanced $BRAF^{V600}$-positive melanoma, Flaherty et al. compared dabrafenib or trametinib monotherapy with the combination of these two drugs [49]. They found that the incidence of complete or partial responses for the combination cohort was 76% while it was 54% for monotherapy groups. Furthermore, median progression-free survival for the combination therapy group was 9.4 months while it was about 5.8 months for the monotherapy groups. Pyrexia (fever) was much more common in the combination cohort when compared with the monotherapy groups (71% vs. 26%). The occurrence of cutaneous squamous cell carcinomas (7% vs. 19%) and hyperkeratosis (9% vs. 30%) was decreased in the combination therapy cohort when compared with the monotherapy group; these results, however, did not achieve statistical significance ($P = 0.09$). The better response to dual therapy may be due to the MEK inhibitor blockade of the paradoxical activation of the MAP kinase pathway produced by dabrafenib. The combination of trametinib and dabrafenib was approved by the FDA for the treatment of $BRAF^{V600E/K}$-driven melanomas in 2014 (www.brimr.org/PKI/PKIs.htm).

Larkin et al. reported on the results of a clinical trial consisting of 495 patients with treatment-naive advanced $BRAF^{V600}$-mutation positive melanoma receiving both cobimetanib and vemurafenib or vemurafenib plus placebo (the control group) [50]. The duration of median progression-free survival (9.9 vs. 6.2 months) and the frequency of complete or partial responses (68% vs. 45%) was better in the dual-therapy group when compared with the control cohort. The incidence of cutaneous squamous cell carcinomas in the combination group was 2% compared with 11% in the control group while the incidence of keratoacanthomas was 1% in the combination group compared with 8% in the vemurafenib-only group. This represents an unusual situation where a combination therapy produced fewer adverse events than a monotherapy [45]. The studies of Flaherty et al. [49] and Larkin et al. [50] demonstrated that the use of the combination of the B-Raf and MEK1/2 inhibitors is more effective than that of B-Raf or MEK1/2 inhibitor monotherapy.

Dummer et al. reported on the results of a clinical trial that involved 577 patients with advanced $BRAF^{V600}$-mutation positive melanoma that was treatment-naive or that had progressed on or after first-line immunotherapy [51]. Patients were assigned randomly to receive either encorafenib once daily with binimetinib twice daily (encorafenib and binimetinib cohort), encorafenib once daily (encorafenib cohort), or vemurafenib twice daily (vemurafenib cohort). With a median follow-up of 16.6 months, median progression-free survival was 7.3 months in the vemurafenib cohort and 14.9 months in the encorafenib and binimetinib cohort. The most common grade 3–4 adverse events seen in the encorafenib and binimetinib group were hypertension in 6% of patients, increased creatine phosphokinase activity (chiefly a muscle enzyme) in 7% of patients, and increased γ-glutamyltransferase activity (a liver enzyme) in 9% of patients. These investigators concluded that encorafenib monotherapy or encorafenib and binimetinib combination therapy showed more favorable efficacy when compared with vemurafenib monotherapy. Furthermore, they inferred that encorafenib and binimetinib together appear to have an improved tolerability profile when compared with encorafenib or vemurafenib alone. As a result of these findings, the FDA approved encorafenib and binimetinib combination therapy for the treatment of $BRAF^{V600E/K}$-positive advanced melanoma in 2018 (www.brimr.org/PKI/PKIs.htm).

The FDA has approved three B-Raf and MEK1/2 inhibitor combinations for the treatment of $BRAF^{V600}$-mutation positive patients with advanced melanomas (about 50% of all advanced melanoma patients): (i) dabrafenib and trametinib, (ii) vemurafenib and cobimetanib, and (iii) encorafenib and binimetinib. The use of these drug combinations is now the standard of care for these melanoma patients [52]. It is unclear whether one of these drug combinations is superior to the others. The choice between vemurafenib and cobimetanib versus dabrafenib and trametinib may depend upon patient-related factors; in the former case, it is the ability to tolerate cutaneous side effects and in the latter case it is the ability to tolerate fever. However, encorafenib–binimetinib seems to have a better toxicity profile, with a much lower incidence of fever and photosensitivity in patients when compared with other two B-Raf–MEK inhibitor combinations [51]. As these studies are continued, perhaps differences in overall survival will be observed. The addition of a MEK inhibitor allows for a greater dose of the B-Raf inhibitor, which increases the overall therapeutic effectiveness.

Besides orally effective protein-kinase inhibitor therapies, the use of intravenous immune checkpoint inhibitors represents an effective melanoma treatment [53,54]. Pembrolizumab is a monoclonal antibody that stimulates an immune response against malignancies by inhibiting the lymphocyte programmed cell death-1 (PD-1) receptor. Nivolumab, which is a human IgG4 anti-PD-1 monoclonal antibody, is another checkpoint inhibitor. In contrast, ipilimumab is a monoclonal antibody that stimulates the immune response by blocking the cytotoxic T-lymphocyte antigen-4 (CTLA-4), which is a regulator of the immune response. Each of these three immune checkpoint inhibitors is approved by the FDA for the treatment of melanomas irrespective of *BRAF* mutation status. For patients with documented $BRAF^{V600}$ mutations, selection between immune checkpoint therapy or targeted therapy is currently challenging because of the absence of results from current

clinical trials comparing the two treatment modalities. These studies show that significant progress has been made in the treatment of advanced/metastatic melanomas and more clinical studies are underway that potentially add to the effectiveness of both immune checkpoint and targeted treatments. Another option to improve therapeutic outcomes is to combine both protein kinase antagonist and CAR (chimeric antigen receptor) T cell or immune checkpoint therapies [55,56]. Initial clinical trials combining targeted therapy and immunotherapy were unsuccessful because of toxicities, but ensuing clinical trials using different strategies are in progress. Moreover, immunotherapy and targeted therapies may be given sequentially or they might be combined. The outcomes of B-Raf/MEK1/2 inhibitor therapy (dabrafenib and trametinib) followed by immunotherapy (nivolumab and ipilimumab), or vice versa, are being studied in an ongoing clinical trial (NCT02224781). ERK1/2 antagonists that are in clinical trials are considered in Section 6.

3. ERK1/2 structures

3.1. Catalytic residues in the amino-terminal and carboxyterminal lobes

Human ERK1 and ERK2, which are 84% identical in their amino acid sequence, share many, if not all, functions [57]. Like nearly all protein kinases, ERK1/2 contain distinctive amino-terminal and carboxyterminal extensions that provide important functional specificity. ERK1 contains an insertion of 17 amino acid residues in its amino-terminal portion. The ERK1/2 family contains an insertion of 32/35 amino acid residues within the protein kinase domain (kinase insert domain) that provides additional operational specificity. Human ERK1 is made up of 379 amino acid residues while rat and mouse ERK1 is made up of 380 residues. Human ERK2 is made up of 360 amino acid residues while the rat and mouse enzymes are made up of 358 residues. There is more variation in ERK1 and ERK2 in a given species that there is among either ERK1 or ERK2 among the three species. Moreover, the human, rat, and mouse enzymes seem to be functionally equivalent.

Like all protein kinases, ERK1/2 have a small N-terminal lobe and large C-terminal lobe that contain several conserved α-helices and β-strands as first described in PKA [58,59]. The small amino-terminal lobe contains a five-stranded antiparallel β-sheet (β1–β5) [60,61]. The small lobe also contains an important regulatory αC-helix that occurs in active or dormant orientations. The amino-terminal lobe contains a glycine-rich (GxGxΦG) ATP-phosphate-binding loop, sometimes termed the P-loop, which is located between the β1- and β2-strands (Fig. 2A and C). The Φ represents a hydrophobic residue, which is tyrosine in human, rat, and mouse ERK1/2. The glycine-rich loop covers and anchors the non-transferable ATP α- and β-phosphates. The β1- and β2-strands overlay the adenine base of ATP. A conserved valine residue follows the glycine-rich loop (GxGxΦGxV56/V39 in human ERK1/2) that interacts hydrophobically with the adenine base of ATP (all residue numbers, unless otherwise noted, correspond to the human isoforms even when experiments were performed with enzymes from other species). The β3-strand contains a conserved AxK sequence, the lysine of which (K71/54 of ERK1/2) helps to anchor the α- and β-phosphates of ATP. A conserved glutamate occurs near the middle of the αC-helix (E88/71 in ERK1/2) in protein kinases. The presence of an electrostatic bond between the β3-strand lysine and the αC-helix glutamate is a prerequisite for the formation of the activated state and corresponds to the "αC_{in}" conformation (Fig. 2A). The αC_{in} conformation is necessary, but it is not sufficient for the expression of full kinase activity. However, the absence of this electrostatic bond indicates that the kinase is inactive and it is called the "αC_{out}" conformation (Fig. 2C). States between the αC_{in} and αC_{out} conformation are called αC-dilated or αC-out–like [62,63]. The carboxyterminus of the αC-helix is anchored to the αC-β4 back loop. The ERK1/2 αC-β4 back loop residues H97/80 and N99/82 of the amino-terminal lobe, in turn, are anchored to the large lobe αE-helix residues Q149/132, R152/135, and Y156/139; this portion of the back loop is the only part of the amino-terminal lobe that dynamically belongs to the carboxyterminal lobe [61].

The large C-terminal lobe is mainly α-helical (Fig. 2A) with eight conserved segments (αD–αI, αEF1, αEF2) [64]. Although the GHI segment can contribute to the tethering of protein substrates and to protein-protein interactions, it is not as dynamic as the activation segment. Active protein kinases also contain four short conserved β-strands (β6-β9). The β6 and β9-strands may be absent in inactive enzyme conformations (Fig. 2C). The β7-strand occurs on the floor of the adenine binding pocket and the second residue of this strand interacts hydrophobically with virtually all ATP-competitive protein kinase antagonists. The primary structure of the β-strands occurs between those of the αE- and αF-strand helices. The C-terminal lobe contains the catalytic residues associated with the phosphoryl transfer from ATP to the ERK1/2 substrates. The C-terminal tail of ERK2 forms a helix that borders the αC-helix (Fig. 2A) and functions to stabilize the active enzyme and contributes to catalysis [65].

Hanks and Hunter identified 12 subdomains (I–VIa, VIb–XI) with

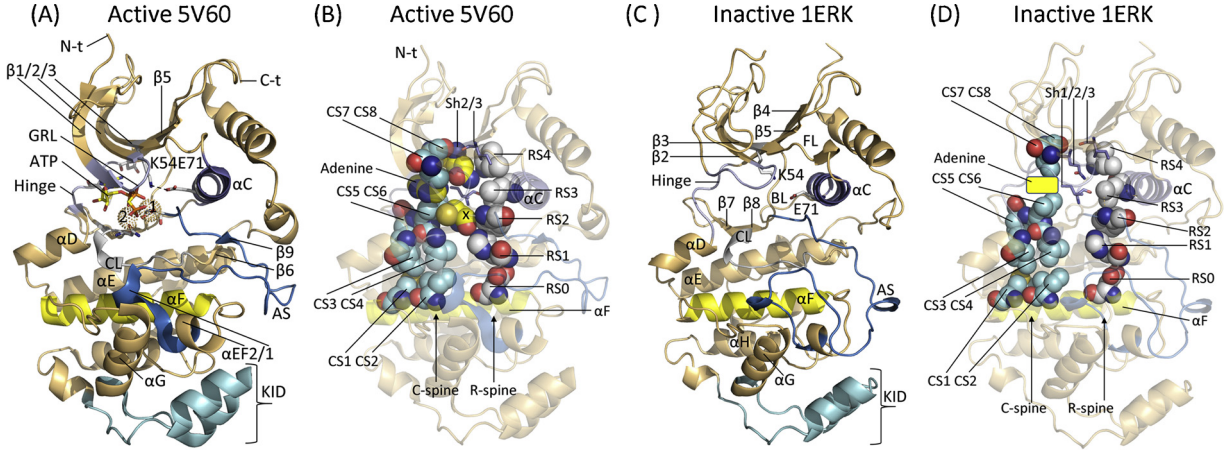

Fig. 2. (A) Diagram of the frontal projection of active ERK2. 1 and 2 label Mg^{+2}(1) and Mg^{2+}(2). ATP occurs below the glycine-rich loop. (B) Depiction of the residues of the active ERK2 C-spine, R-spine, gatekeeper, and x of the xDFG motif shown as spheres. The carbon atoms of the gatekeeper and xDGF-x are yellow. (C) Inactive ERK2. (D) Spine and shell residues of inactive ERK2. The PDB ID is given in the title. The carbon atoms of the C-spine are sky gray, those of the R-spine are cyan; the shell residues are shown in a stick format with carbon atoms in dark blue. The dashed lines represent a hydrogen bond. AS, activation segment; BL, αC-β4 back loop; C-t, C-terminal end; CL, catalytic loop; FL, β3-αC front loop; KID, kinase insert domain; GRL, glycine-rich loop; N-t, N-terminal end. Figs. 2,3, and 6 were prepared using the PyMOL Molecular Graphics System Version 1.5.0.4 Schrödinger, LLC.

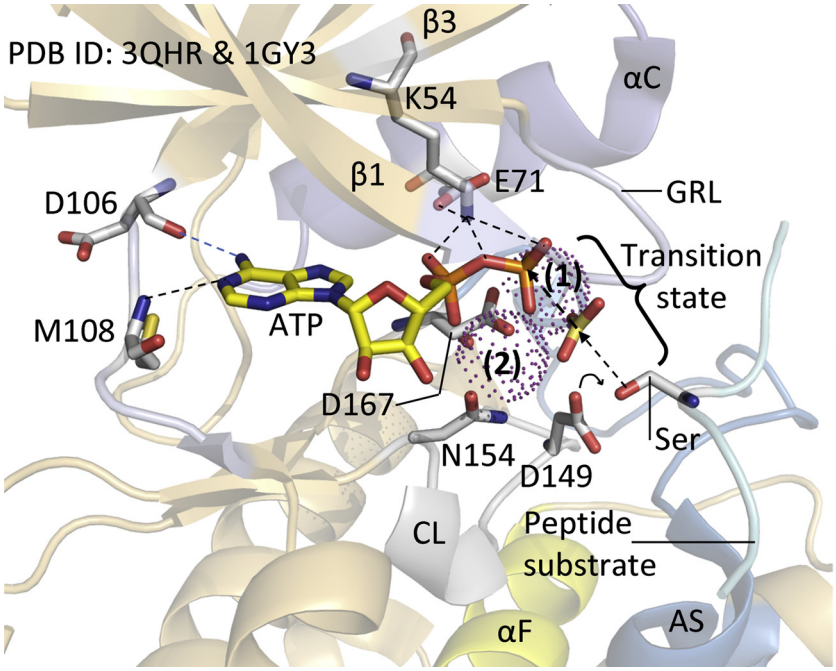

Fig. 3. Inferred mechanism of the ERK-catalyzed protein kinase reaction. HRD-D149 abstracts a proton from the protein-serine substrate allowing for its nucleophilic attack onto the γ-phosphorus atom of ATP. 1 and 2 label the two Mg^{2+} ions shown as dots. AS, activation segment. The figure was prepared from PDB IDs 3QHR 1GY3 corresponding to human CDK2, but the residues correspond to those of human ERK2.

conserved amino acid residue signatures that make up the catalytic core of protein kinases [66]. Of these, the following four amino acids, which define a K/E/D/D (Lys/Glu/Asp/Asp) motif, illustrate the catalytic properties of ERK1/2. A conserved β3-strand lysine (K71/54 in ERK1/2, the *K* of *K*/E/D/D) forms salt bridges with the α- and β-phosphates of ATP (Fig. 3). The *E* of K/*E*/D/D is the αC-helix glutamate that forms an electrostatic bond with the β3-strand lysine. Asp166/149, which are Lowry-Brönsted bases (proton acceptors) occurring within the catalytic loop, play an important role in catalysis; this aspartate is the first *D* of K/E/*D*/D. Gibbs and Zoller observed that mutation of the equivalent residue in yeast PKA resulted in a k_{cat} (0.05 s^{-1}) that was about 0.3% that of the wild-type enzyme (16.9 s^{-1}) [67]. Madhusudan et al. inferred that this aspartate abstracts the proton from the −OH group of the protein substrate thereby enabling the nucleophilic attack of oxygen on the γ-phosphorus atom of ATP [68]. Furthermore, Zhou and Adams suggested that this aspartate places the substrate hydroxyl group in a position that enables an in-line nucleophilic attack [69]. See Ref. [70] for an overview of the enzymology of protein kinases.

The second *D* of the K/E/D/*D* signature, Asp184/167, is the first residue of the activation segment. The activation segment, which is generally 35–40 residues long, is one of the most important regulatory elements in protein kinases [71]. This segment influences both protein substrate binding and overall catalytic efficiency. The activation segments of nearly all protein kinases begin with DFG and the segments of most protein kinases including ERK1/2 end with APE. The primary structure of the catalytic loop of ERK2, which is proximal to the β6- and β7-strands, consists of HRDLKPSN. The primary structure of the activation segment occurs after that of the catalytic loop and before that of the αF-helix. Waas and Dalby reported that two Mg^{2+} ions – Mg^{2+}(1) and Mg^{2+}(2) – are required for the catalytic activity of rat ERK2 [72]. The activation segment DFG-D binds to one magnesium ion – Mg^{2+}(1) – while the catalytic loop HRD(x)$_4$N-asparagine binds to the second magnesium ion – Mg^{2+}(2). Mg^{2+}(1) interacts with the α- and β-phosphates of ATP while Mg^{2+}(2) generally interacts with the α- and γ-phosphates of the nucleotide.

The middle of the activation segment, which is its most diverse part in various protein kinases in terms of length and sequence, is known as the activation loop in protein kinases in general, but as the activation lip in ERK2 [65,73]. This segment in ERK1/2 contains a phosphorylatable tyrosine that is two residues downstream from a phosphorylatable threonine. Both covalently bound phosphates are required to maintain the high activity state. The beginning of the activation segment is near the amino-terminus of the αC-helix and the conserved HRD component of the catalytic loop. Although the αC-helix belongs to the amino-terminal lobe, it occupies a strategically important position between the two lobes. The negatively charged tyrosine and threonine phosphates serve as structural organizers of the active site [73]. ERK2 pY187 forms the proline-directed specificity pocket. In the dormant unphosphorylated enzyme state, the activation segment (lip) is folded to block the proline-binding site. The ERK2 pT185 phosphate forms a salt bridge with R70 of the αC-helix that enables the formation of the αC-helix E71 and the β4-strand K54 polar bond corresponding to the αC_{in} active state.

ERK1/2 catalyze the phosphorylation of protein-substrate serine/threonine residues that occur in the sequence S/T-P [74]. Proline at the P + 1 position is a consistent primary sequence determinant of ERK1/2 substrates. The phosphorylation site is labeled 0 (zero), the residue immediately after the phosphorylation site is labeled +1, and the residue immediately before the phosphorylation site is labeled –1. The propensity for proline at the P + 1 site arises from the structure of the ERK1/2 activation segment protein-binding site. Several protein kinases such as PKA contain a pocket for a large hydrophobic residue immediately following the phosphorylatable serine or threonine residue [75,76]. However, the X-ray crystal structure of activated ERK2 shows a shallow surface depression at the site where the ERK2 phosphotyrosine occupies the pocket seen in other kinases [73,77]. Proline is the preferred P + 1 substrate component because its preferred backbone structure places the side chain away from the kinase surface lacking the hydrophobic-residue–binding pocket. Using synthetic peptides as substrates, a detailed analysis of substrate specificity reveals that PxS/TP represents the optimal primary sequence for ERK1/2 phosphorylation with proline at the +1 and –2 positions [74].

ERK1/2 interact with two separate docking domains (D-site and F-site) that occur within their protein substrates, their proximal activating enzymes, and their inactivating phosphatases. ERK1/2 contain a D-site recruitment site (DRS) that binds to the D-site docking domain of substrates and an F-site recruitment site (FRS) that binds to the F-site docking domain of substrates. Some substrates possess both docking sites while others have a D-docking site or an F-docking site [78]. The D-site recruitment site of ERK1/2 occurs on the back of the enzyme as

usually viewed; it contains a hydrophobic component and a negatively charged region. The F-site recruitment site of ERK1/2, which binds to a substrate F-docking site, occurs in front of the enzyme near the activation segment. The F-site was first characterized as an FxFP sequence that was found in ERK1/2 substrates [78]. This site is conserved in several ERK1/2 interacting proteins including (i) the transcription factors c-Fos, Sap1, Elk1, Lin1, (ii) dual specificity protein phosphatases such as MKP1 (DUSP1) and MKP4 (DUSP4), and (iii) the kinase suppressor of Ras (KSR) [78,79]. In contrast to most protein kinases with only an activation segment protein-substrate recognition sequence, we observe that ERK1/2 possess two additional protein-substrate recognition sequences. See Ref. [19] for a summary of the location, structure, and properties of the substrate docking sites and the ERK1/2 recruitment sites.

The activation segment exhibits an extended or open conformation in all active enzymes and closed conformation in many dormant enzymes. The first two residues of the activation segment of various protein kinases exist in two different conformations. In the dormant activation segment conformation of many protein kinases, DFG-D extends away from the active site. This is called the "DFG-D_{out}" conformation. The aspartate side chain of active protein kinases extends toward the ATP-binding pocket and coordinates Mg^{2+}(1). This corresponds to the "DFG-D_{in}" conformation. It is the ability of aspartate to bind (DFG-D_{in}) or not bind (DFG-D_{out}) to Mg^{2+}(1) in the active site that is significant. The DFG-D_{out} conformation is much more common in protein-tyrosine kinases than protein-serine/threonine kinases [80]. See Ref. [81] for details concerning these two activation segment conformations. However, the inactive conformations of ERK1/2 exist in the DGF-D_{in} conformation with a closed activation segment, with an αC_{out} conformation, with an altered glycine-rich loop, or a combination of these configurations. Functionally important ERK1/2 residues are listed in Table 1.

3.2. The ERK1/2 protein kinase hydrophobic skeletons

Kornev et al. [82,83] analyzed the structures of active and inactive conformations of two dozen protein kinases and determined functionally important residues by a local spatial alignment algorithm. This analysis reveals a structure of eight hydrophobic residues that constitute a catalytic or C-spine and four non-consecutive hydrophobic residues that constitute a regulatory or R-spine. Each spine consists of residues derived from both the N- and C-terminal lobes. The spines provide a firm, but flexible, connection between the lobes. The R-spine contains residues from the activation segment and the αC-helix, whose conformations are important in defining active and inactive states. The C-spine governs catalysis by directing ATP binding. The C-spine dictates the positioning of ATP and the R-spine interacts with the protein substrate enabling catalysis. The proper alignment of the spines is necessary, but it is not sufficient, for the assembly of an active protein kinase.

The ERK1/2 regulatory spines consist of a residue from the beginning of the large lobe catalytic loop HRD-histidine (H164/147), from the large lobe activation segment DFG-F (F185/168), from the C-terminal end of the small lobe αC-helix (L92/75), and from the small lobe β4-strand (I103/86). L92/75 and comparable residues from other protein kinases are four residues C-terminal to the conserved αC-helix glutamate. The backbone of H164/147 is anchored to a conserved aspartate residue (D227/210) in the αF-helix by a hydrogen bond. Meharena et al. named the R-spine residues RS0, RS1, RS2, RS3, and RS4 going from the base to the apex [84]. We named the catalytic spine residues going from the bottom to the top as CS1–8 [85].

Table 2 lists the residues of the spines in human and rat ERK1and ERK2 and the catalytic subunit of murine PKA and Fig. 2B and D shows the location of the catalytic and regulatory spines of active human and dormant rat ERK2, respectively. Although K54 and E71 of dormant ERK2 fail to form a salt bridge, surprisingly, the R-spines in active ERK2 and inactive ERK2 are linear and nearly superimposable (Fig. 2C). See Refs. [86,87] for a summary of the properties of the spine residues of the ALK receptor protein-tyrosine kinase, Refs. [88,89] for those of the CDK (cyclin-dependent kinase) family of protein/serine kinases, Ref. [90–92] for those of the EGFR family of protein-tyrosine kinases, Ref. [93] for those of the Janus kinase (JAK) non-receptor protein-tyrosine kinases, Ref. [94] for those of the Kit receptor protein-tyrosine kinase, Ref. [17] for those of the MEK1/2 dual-specificity protein kinases, Ref. [95] for those of the PDGFRα/β protein-tyrosine kinases, Refs. [12,16] for those of the RAF protein-serine/threonine kinase, Ref. [96] for those of the RET receptor protein-tyrosine kinase, Ref. [97] for those of the ROS1 orphan receptor protein-tyrosine kinase, Refs. [98,99] for those of the Src non-receptor protein-tyrosine kinase, and Ref. [100] for those of the VEGFR1/2/3 protein-tyrosine kinases. The importance of the interaction of therapeutic protein kinase antagonists with the C- and R-spine residues cannot be overemphasized as documented in these citations.

The catalytic spine of protein kinases consists of two residues from the small lobe and six residues from the large lobe (Fig. 2B). The binding of the adenine base of ATP in its binding pocket brings the two parts of the C-spine together, allowing the two lobes of the enzyme to

Table 1
Important residues in the human and rat ERK1/2.

	Human ERK1	Human ERK2	Rat ERK1	Rat ERK2	Inferred function
Protein kinase domain	42–330	25–313	43–331	23–311	Catalyzes substrate phosphorylation
Glycine-rich loop GEGAYG	49–54	32–37	50–55	30–35	Anchors ATP α- and β-phosphate
The β3-lysine or the *K* of *K*/E/D/D	71	54	72	52	Forms salt bridges with ATP α- and β-phosphates and with αC-E
The αC-glutamate, or the *E* of K/*E*/D/D	88	71	89	69	Forms salt bridges with β3-K
Hinge residues	123–126	106–109	124–127	104–107	Connects N- and C-lobes
Gatekeeper residue	Q122	Q105	Q123	Q103	Stabilizes enzyme & limits access to back pocket
Catalytic loop HRDLKPSN	164–171	147–154	165–172	145–152	Plays both structural and catalytic roles
Catalytic HRD	164–166	147–149	165–167	145–147	Beginning of the catalytic loop
Catalytic HRD-*D* and the *D* of K/E/*D*/D	166	149	167	147	Catalytic base
Catalytic loop $HRD(x)_4N$-*N*	171	154	172	152	Chelates Mg^{2+}(2)
Activation segment DFG-*D* and the second *D* of K/E/D/*D*	184–186	167–169	185–187	165–157	Chelates Mg^{2+}(1)
Activation segment phosphorylation sites	T202, Y204	T185, Y187	T203, Y205	T183, Y185	Phosphorylation required for activation
APE at the end of the activation segment	212–214	195–197	213–215	193–195	Interacts with the αHI loop and stabilizes the activation segment
Kinase insert domain (KID)	257–291	243–274	258–292	241–272	Binds substrates with FxFP motif
No. of residues	379	360	380	358	
Molecular Weight (kDa)	43.1	41.4	40.0	41.3	
UniProtKB accession no.	P27361	P28482	Q63844	P63086	

Table 2
Human and rat ERK1/2 spine and shell residues.

	Symbol	KLIFS No.[a]	Human ERK1/2	Rat ERK1/2	Murine PKA[b]
Regulatory spine					
β4-strand (N-lobe)	RS4	38	I103/86	I104/84	L106
αC-helix (N-lobe)	RS3	28	L92/75	L93/73	L95
Activation loop DFG-F (C-lobe)	RS2	82	F185/168	F186/166	F185
Catalytic loop HRD-H/Y (C-lobe)[b]	RS1	68	H164/147	H165/145	Y164
αF-helix (C-lobe)	RS0	None	D227/210	D228/208	D220
Shell residues					
Two residues upstream from the gatekeeper	Sh3	43	I120/103	I121/101	M118
Gatekeeper, end of the β5-strand	Sh2	45	Q122/105	Q123/103	M120
αC-β4 back loop	Sh1	36	I101/84	I102/82	V104
Catalytic spine					
β3-strand A of the AxK motif (N-lobe)	CS8	15	A69/52	A70/50	A70
β2-strand V (N-lobe)	CS7	11	V56/39	V57/37	V57
β7-strand (C-lobe)	CS6	77	L173/156	L174/154	L173
β7-strand (C-lobe)	CS5	76	L172/155	L173/153	L172
β7-strand (C-lobe)	CS4	78	I174/L157	I175/L155	I174
αD-helix (C-lobe)	CS3	53	L129/112	L133/113	M128
αF-helix (C-lobe)	CS2	None	I234/217	I235/215	L227
αF-helix (C-lobe)	CS1	None	M238/221	M239/219	M231

[a] Ref. [122].
[b] Refs. [82–84].

close [83,101]. The assembly of the C-spine poises the enzyme for catalysis. The two residues of the small lobe of ERK1/2 that bind to the adenine component of the nucleotide substrate include the conserved valine within GxGxΦGxV56/39 (CS7) of the β2-strand and A69/52 (CS8) from the conserved AxK motif of the β3-strand. Moreover, L173/156 (CS6) from the middle of the β7-strand interacts hydrophobically with the adenine base in the active enzyme. L172/155 (CS5) and I174/L157 (CS4), hydrophobic residues that flank L173/156 (CS6), interact with L129/112 (CS3) at the beginning of the αD-helix. The αD-helix CS3 residues interact hydrophobically with the adjacent I174/L157 (CS4) and M238/221 (CS1) of the αF-helix. Both the C-spine and R-spine interact with the hydrophobic αF-helix, which serves as a central scaffold for the assembly of the entire protein kinase molecule. Besides the hydrophobic interactions with the adenine moiety, the exocyclic 6-amino nitrogen of ATP characteristically forms a hydrogen bond with a backbone residue in the hinge that connects the small and large lobes. Most small-molecule inhibitors of protein kinases that compete with ATP binding also make hydrogen bonds with the backbone residues of the hinge [85].

Using site-directed mutagenesis, Meharena et al. described three residues in murine PKA that stabilize the R-spine, which they labeled Sh1, Sh2, and Sh3 (Sh refers to shell) [84]. The Sh1 V104 G mutant had 5% of the catalytic activity of wild type PKA while the Sh2/Sh3 M120 G/M118 G double mutant was completely inactive. These results suggest that the shell residues promote an active protein kinase structure. The Sh1 residue of protein kinases is located in the αC-β4 back loop. The Sh2 or gatekeeper occurs at the end of the β5-strand immediately before the hinge, and Sh3 occurs two residues upstream from the gatekeeper in the β5-strand.

The name gatekeeper denotes the role that this residue plays in controlling access to a hydrophobic pocket next to the adenine binding site [102,103] that is occupied by portions of many small molecule protein kinase antagonists. Based upon the local spatial pattern alignment data [84], only three of the 14 amino acid residues in PKA surrounding RS3 and RS4 are conserved. These shell residues stabilize and strengthen the protein kinase regulatory spine. To reiterate, many therapeutic ATP-competitive steady-state protein kinase inhibitors interact with catalytic spine (CS6/7/8), shell (Sh1 and Sh2), and regulatory spine (RS1/2/3) residues. The gatekeeper residue in ERK1/2 is glutamine 122/105 and this residue is found in the Sh2 position (the P20 residue) in about eight protein kinases making it an uncommon gatekeeper residue [104]. About 77% of human protein kinases have a relatively large (e.g., Leu, Met, Phe) residue in this position while the remainder have smaller gatekeeper residues (e.g., Thr, Val).

3.3. Phosphorylation and activation of ERK1/2

A portion of the protein kinase catalytic site lies in the deep cleft between the amino-terminal and carboxyterminal lobes. In the catalytically inactive form of the enzyme, the lobes are modestly tilted away from each other. In the catalytically active form of the enzyme, the lobes are closer together, but the two lobes of protein kinases are able to move relative to one another during the catalytic cycle; this movement allows for the binding of ATP and the release ADP [75]. In the case of rat ERK2, the lobes rotate 5.4° closer when going from the unphosphorylated dormant to the phosphorylated active conformation [65,73]. After the ATP and protein substrate bind, additional changes in the closed enzyme bring residues into the catalytically active state facilitating the phosphoryl transfer from ATP to the protein substrate (Fig. 3). The αC-helix is bound to the small lobe β-sheet core and the lobe moves as a rigid body that opens and closes as part of the catalytic cycle. The catalytic loop contains most of the catalytic machinery while the DFG-D plays the important role of binding Mg^{2+}(1).

The conversion of dormant ERK1/2 to the active enzyme form requires the phosphorylation of two residues within the activation loop as catalyzed by MEK1/2. These two residues occur in the sequence Thr-Glu-Tyr (T-E-Y). All MAP kinases contain a Thr-Xxx-Tyr sequence in their activation segment; the p38 isoforms contain Thr-Gly-Tyr and the JNK isoforms contain Thr-Pro-Tyr. MEK1/2 first catalyze the phosphorylation of the tyrosine residue in the ERK1/2 activation segments [105,106]. Then tyrosine-phosphorylated ERK1/2 dissociates from MEK1/2 and subsequently re-associates with the same or another active MEK1/2 that then catalyzes the phosphorylation of the activation-segment threonine, which is two residues upstream from the ERK1/2 phosphotyrosine [105–107]. Anderson and colleagues [108] discovered that ERK2 can be completely deactivated by treatment with either CD45 – a protein phosphatase specific for phosphotyrosine [109], or by phosphatase 2 A – a protein phosphatase specific for phosphoserine/threonine [110,111]. Furthermore, they demonstrated that MAP kinase is fully active only when both the tyrosyl and threonyl residues are phosphorylated. Taylor et al. refer to the process of going from the dormant to active conformation (and vice versa) as a dynamic molecular switch [112].

4. Classification of protein kinase-drug complexes

Dar and Shokat described three categories of protein kinase inhibitors and classified them as types I, II, and III [103]. Accordingly, type I antagonists bind in the adenine-binding pocket of an active protein kinase; type II antagonists bind to an inactive protein kinase with the activation segment DFG-D pointing away from the active site (DFG-D_{out}); type III antagonists bind to an allosteric site that is separate from the adenine-binding pocket. Zuccotto later defined type I½ antagonists as drugs or ligands that bind to an inactive protein kinase with the activation segment DFG-D directed inward (DFG-D_{in}) toward the active site (in contrast to the DFG-D_{out} conformation of type II inhibitors) [113]. An inactive protein kinase may display a closed activation segment, an αC_{out} conformation, a nonlinear or broken regulatory spine, an abnormal glycine-rich loop, or various combinations thereof. Gavrin and Saiah then divided allosteric inhibitors into types III and IV [114]. Type III inhibitors bind within the cleft between the amino-terminal and carboxyterminal lobes and next to, but independent of, the ATP binding site while type IV inhibitors bind outside of the cleft that connects the small and large lobes. Furthermore, Lamba and Gosh defined bivalent antagonists as those inhibitors that span two distinct regions of the protein kinase domain as type V inhibitors [115]. For example, an antagonist that bound to the adenine-binding pocket as well as the SH2 domain of Src would be classified as a type V inhibitor [116]. To complete this taxonomy, we labeled antagonists that bind covalently with their target enzyme as type VI inhibitors [85]. For example, afatinib is a covalent type VI inhibitor of mutant EGFR that is used for the treatment of NSCLC. Mechanistically, this drug initially binds to an active EGFR conformation (like a type I inhibitor) and then the C797 –SH group of the receptor attacks the drug to form an irreversible covalent adduct (PDB ID: 4G5J) [85].

Owing to the multitude of inactive protein kinase conformations when compared with the conserved active conformation, it was surmised that type II inhibitors would be more selective than type I inhibitors, which bind to a conserved active conformation. The analysis of Vijayan et al. support this proposal [62] while those of Zhao et al. and Kwarcinski et al. do not [117,118]. By definition, type III allosteric inhibitors bind adjacent to the adenine binding pocket [114]. Because of the greater variability of this region when compared with the adenine-binding site, type III inhibitors have the potential to possess greater selectivity than type I, I½, or II inhibitors. Furthermore, Kwarcinski et al. suggested that inhibitors that bind to the αC_{out} conformation (type I½ inhibitors) may be more selective than type I or II antagonists [117]. Abemaciclib, palbociclib, and ribociclib (all CDK4/6 antagonists) are FDA-approved αC_{out} inhibitors. However, Kwarcinski et al. inferred that not all protein kinases are able to assume the αC_{out} conformation while they suggested that all protein kinases are able to adopt the DFG-D_{out} conformation [117]. In contrast, Hari et al. provided evidence that many kinases are unable to adopt the DFG-D_{out} conformation [80]. A tally of more than 1250 protein kinase X-ray crystal structures in 2014 indicated that 85% of them have a DFG-D_{in} conformation, 10% have a DFG-D_{out} conformation, and 5% have a DFG-D dilated or out-like conformation [62,63]. They also reported that 55% of protein kinase structures exhibit the αC-helix in structure, 33% have the αC-helix out structure, and 11% have an αC-helix dilated or out-like structure. Thus far, wildtype ERK1/2 structures have not been observed with the DFG-D_{out} conformation [80].

We previously divided type I½ and type II inhibitors into A and B subtypes [85]. Agents that extend into the back cleft past the gatekeeper residue are classified as type A inhibitors. In contrast, drugs that do not extend into the back pocket as are classified as type B inhibitors. Based upon incomplete findings, the possible significance of this difference is that type A inhibitors may bind to their target enzyme with longer residence times [119] as compared with type B inhibitors [85]. Sorafenib is a multikinase and VEGFR type IIA inhibitor that is approved by the FDA for the treatment of renal cell carcinomas [85]. Sunitinib is a multikinase and VEGFR type IIB inhibitor that is also approved by the FDA for the treatment of renal cell carcinomas. The former has a residence time of 64 min while that of the latter has a residence time of less than 2.9 min.

Ung et al. studied a variety of structural features using the location of the DFG-motif and the αC-helix to define the conformational space of the protein kinase catalytic domain [120]. Their studies describe the movement of the DFG motif from its active DFG-D_{in} location to the dormant DFG-D_{out} location. Correspondingly, the αC-helix can move from its active αC_{in} location to the dormant αC_{out} position by tilting and rotating. These investigators enumerated five different protein kinase structures; these include (i) αC_{in}-DFG-D_{in} (CIDI), (ii) αC_{out}-DGF-D_{in} (CODI), (iii) αC_{in}-DFG-D_{out} (CIDO), (iv) αC_{out}-DFG-D_{out} (CODO), and (v) ωCD; the latter designation denotes structures with variable αC-helix or DFG-D locations. CIDI designates the catalytically active conformation with a linear R-spine. In contrast, CIDO has the DFG-D 180° rotation that creates a new hydrophobic pocket and displaces DFG-F outward resulting in the fracture of the R-spine. CODI denotes the αC_{out} and DFG-D_{in} configuration. This may ensue as a result of the activation loop shifting the αC-helix to the αC_{out} position. Alternatively, a drug or ligand may move the αC-helix outward. The CODO conformation is rarely observed. ωCD structures represent a heterogeneous group with variable αC-helix positioning and diverse DFG-D intermediate states. Moreover, Ung et al. hypothesize that the ωCD states represent transitions among the various primary configurations [120].

5. Drug-ligand binding pockets

Liao [121] and van Linden et al. [122] partitioned the region between the protein kinase amino-terminal and carboxyterminal lobes into the front cleft (front pocket), the gate area, and the back cleft. The gate area and back cleft signify the back pocket or hydrophobic pocket II (HPII) (Fig. 4). The front cleft includes the hinge residues, the adenine-binding pocket, the glycine-rich loop and the catalytic loop (HRD $(x)_4N$) residues. The gate area includes the β3-strand of the N-terminal lobe and the proximal section of the activation segment including DFG of the C-terminal lobe. The back-cleft extends to the αC-β4 loop, to

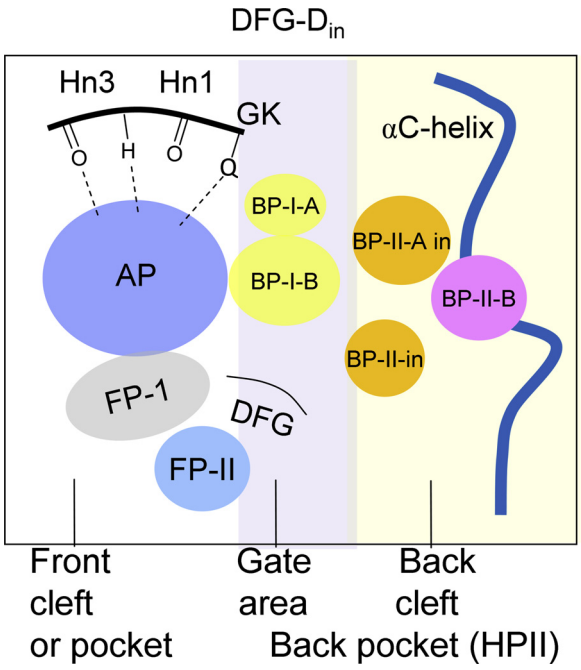

Fig. 4. Location of the protein kinase domain drug-binding pockets. AP, adenine pocket; BP, back pocket; FP, front pocket; Hn, hinge; HPII, hydrophobic pocket II. Adapted from Ref. [122].

Table 3
Location of selected catalytic cleft residues.

Description	Location	KLIFS residue no.[a]
GxGxΦG	Front cleft	4–9
β2-strand V (CS7)	Front cleft	11
β3-strand A (CS8)	Front cleft	14,15
HRD with DFG-D_{in}	Front cleft	68–70
HRD$(x)_4$N-N	Front cleft	75
β7-strand CS6	Front cleft	77
Gatekeeper	Gate area	45
β3-strand K three residues before αC-helix	Gate area	17
αC-β4 penultimate back loop residue	Gate area	36
The x of xDFG	Gate area	80
DFG	Gate area	81–83
αC-helix E	Back cleft	24
RS3	Back cleft	28
HRD with DFG-D_{out}	Back cleft	68–70

[a] Ref. [122].

portions of the β4- and β5-strands of the small lobe, and to a section of the αE-helix within the large lobe. One of the difficulties in the design of effective small molecule protein kinase inhibitors is to provide selectivity that reduces unwanted off-target side effects [63], a process that is aided by examining protein kinase-drug interactions [42,123,124]. The binding pockets in the catalytic cleft play important roles that are related to drug affinity and protein kinase inhibitor design. Hydrogen bonding and halogen bonding [125] also serve to increase ligand-binding affinity. An important strategy to increase drug-binding affinity is to exploit hydrophobic interactions, many of which are described in Section 6.

van Linden et al. described several components that are found in the front cleft, gate area, and back cleft (Table 3) [122]. Accordingly, the front cleft contains an adenine-binding pocket (AP) and two front pockets (FP-I and FP-II). The majority of ATP-competitive inhibitors use a core scaffold to recognize key pharmacophoric features of the adenine binding pocket. This scaffold is decorated with various chemical moieties that extend into adjacent binding pockets. FP-I occurs between the solvent-exposed hinge residues and the C-terminal lobe xDFG-motif (where x is the amino acid residue immediately before the activation segment DFG) and FP-II occurs between the glycine-rich loop and the small lobe β3-strand at the ceiling of the cleft. BP-I-A and BP-I-B occur within the gate area between the β3- and β4-strands, the conserved β3-strand K of the AxK signature, and the αC-helix of the N-terminal lobe and the xDFG-motif of the C-terminal lobe. The smaller BP-I-A pocket occurs at the top of the gate area and it is enclosed by residues of the β3- and adjacent β5-strands including the β3-AxK residues and the regulatory αC-helix. The larger BP-I-B is found in the center of the gate area allowing for access to the back cleft. Both BP-I-A and BP-I-B are found in both the DFG-D_{in} and DFG-D_{out} conformations. The x residue of the xDFG signature as well as the gatekeeper residue serves to connect the C- and R-spines (Fig. 2B) [122].

BP-II-A-in and BP-II-in are found within the back cleft of the DFG-D_{in} conformation [121]. These sub-pockets are enclosed by the C-terminal lobe DFG-motif and the N-terminal lobe αC-helix, αC-β4 back loop, and the β5- and β4-strands. A major modification of BP-II-A-in and BP-II-in creates BP-II-out that is found in the DFG-D_{out} configuration (not shown); this structural transformation results from the movement of DFG-F. The newly formed region is called back pocket II-out (BP-II-out); it occurs where the DFG-F is located in the DFG-D_{in} configuration. BP-II-B is bordered by the αC-helix and the adjacent β4-strand in both the DFG-D_{in} and DFG-D_{out} conformations. Back pocket III (BP-III) occurs only in the DFG-D_{out} conformation. Because ERK1/2 fail to assume the DFG-D_{out} structure, other components of its pockets and subpockets are not considered here; see Refs. [122,123] for further information.

van Linden et al. developed a comprehensive descriptor of ligand and drug binding to more than 1200 human and mouse protein kinase domains [122]. Their KLIFS (kinase–ligand interaction fingerprint and structure) catalogue includes an alignment of 85 potential ligand binding-site residues occurring in both the N-terminal and C-terminal lobes; this catalogue facilitates the classification of ligands and drugs based upon their binding characteristics and it helps in the detection of related interactions. Moreover, these authors devised a uniform amino acid residue numbering system that facilitates the comparison of different protein kinases. Table 2 specifies the correspondence between the catalytic spine, shell, and regulatory spine amino acid residue nomenclature and the KLIFS database residue numbers. Furthermore, these investigators established a helpful free and searchable web site that is regularly updated that provides valuable information on the interaction of human and mouse protein kinases with ligands and drugs (klifs.vu-compmedchem.nl/). At the end of 2018, the data base included more than 4500 PDB structures. Additionally, Carles et al. established a comprehensive directory of protein kinase inhibitors in clinical trials [126]. They developed a free and searchable web site that is regularly updated which includes inhibitor structures and their physical properties, protein kinase targets, therapeutic indications, year of first approval (if applicable), and trade name (http://www.icoa.fr/pkidb/). The Blue Ridge Institute for Medical Research website, which is regularly updated, depicts the structures and properties of all small molecule protein kinase inhibitors that are approved by the FDA (www.brimr.org/PKI/PKIs.htm).

6. Selected ERK1/2 inhibitors that are in clinical trials

Owing to the frequency of MAP kinase-driven malignancies, it is not surprising that many clinical trials are related to inhibition of this hierarchical three-tiered pathway. More than 300 clinical trials are related to Raf inhibition (clinicaltrials.gov). The relevant diseases include breast, colorectal, renal cell, and other solid tumors, gliomas, melanomas, and NSCLC. *KRAS* mutant colorectal cancers, esophageal squamous cell carcinomas, and head and neck squamous cell carcinomas have also been targeted by Raf inhibitors. Additionally, more than 300 clinical trials are related to the inhibition of MEK1/2. Disease targets include those listed for the Raf inhibitor clinical trials with the addition of pancreatic, prostate, and thyroid cancers, gastrointestinal stromal tumors, various leukemias, and rheumatoid arthritis. ERK1/2 monotherapy or a combination of ERK1/2 inhibitors with MEK1/2 or Raf inhibitors has the potential to expand the types of neoplasms that can be treated with MAP kinase pathway-driven tumors. In contrast to the large number of clinical trials involving Raf and MEK antagonists, only about 35 clinical trials are related to the inhibition of ERK1/2 (Table 4).

Ulixertinib is an orally effective pyridine-pyrrole derivative (Fig. 5A) that is under clinical evaluation for the treatment of advanced solid tumors, pancreatic cancers, acute myelogenous leukemias, and non-Hodgkin lymphomas. Germann et al. reported that the drug is a potent ATP-competitive inhibitor of ERK1/2 with a K_i values of 0.3/0.04 nM, respectively [127]. They reported that pERK1/2 levels increased in various cancer cell lines in a concentration-dependent fashion after 4 and 24 h of ulixertinib treatment. Despite prominent concentration-dependent increases in pERK1/2 observed with 2 μM ulixertinib treatment, phosphorylation of RSK1/2 (an ERK1/2 protein substrate) was reduced at both 4 and 24 h, which is consistent with sustained ERK1/2 inhibition. Total levels of DUSP6, the transcription of which is regulated by ERK1/2, were also attenuated at 4 and 24 h. The biosynthesis of DUSP6 represents a delayed negative feedback mechanism that results in the dephosphorylation of pERK and its inactivation. In resting cells, ERK1/2 is found chiefly in the cytoplasm. However, after phosphorylation, pERK1/2 migrates to the nucleus where transcriptional factors are activated [19]. Treatment with ulixertinib resulted in elevated pERK1/2 levels in the nucleus and cytoplasm. Despite increased pERK1/2 in both compartments, pRSK levels

Table 4
Properties of selected orally effective ERK1/2 inhibitors that are in clinical trials (clinicaltrials.gov).

Drug (Code)	PubMED CID	Formula	MW (Da)	H bond D/A[a]	cLogP[b]	LipE[c]	LE[d]	No. of clinical trials
Ulixertinib (BVD-523)	11719003	$C_{21}H_{22}Cl_2N_4O_2$	433.3	4/4	3.598	5.79 [127] [e]	0.457	8, 3 completed, 5 recruiting
(MK-8353)	58282870	$C_{37}H_{41}N_9O_3S$	691.9	2/9	4.539	3.62 [129] [e]	0.230	3, 2 recruiting, 1 terminated
Ravoxertinib (GDC-0994)	71727581	$C_{21}H_{18}ClFN_6O_2$	440.9	2/7	2.408	6.10 [131] [e]	0.400	2, completed
(SCH772984)	24866313	$C_{33}H_{33}N_9O_2$	587.7	2/8	2.831	6.19 [132] [e]	0.288	None
(Compound **27**)	None	$C_{29}H_{32}ClN_5O_4$	529.2	3/7	2.892	6.63 [133] [e]	0.308	None
(CC-90003)	90331177	$C_{22}H_{21}F_3N_6O_2$	458.4	3/7	4.186	?	?	1, terminated
(KO-947)	136653617	$C_{21}H_{17}N_5O$	355.4	2/5	2.584	?	?	1, recruiting
(LY3214996)	121408882	$C_{22}H_{27}N_7O_2S$	453.6	1/7	2.512	?	?	1, recruiting
(LTT-462)	None	?	?	?	?	?	?	2, recruiting
(LY3214006)	None	?	?	?	?	?	?	1, recruiting
(ONC201)	None	?	?	?	?	?	?	18, 14 recruiting, 1 active, 1 completed, 2 suspended

[a] D/A, donor/acceptor.
[b] cLogP, calculated log of the partition coefficient using MedChem Designer^{TM} version 2.0 Simulationsplus, Inc. Lancaster CA 93534, USA.
[c] LipE (lipophilic efficiency) = pIC_{50} – cLogD where cLogD, the calculated log of the distribution coefficient, was obtained using MedChem Designer^{TM}.
[d] LE (ligand efficiency) = $-2.303 \log_{10} K_{eq}$/N where N is the number of heavy (non-hydrogen) atoms in the drug.
[e] Source of the data for calculating LipE and LE.

are lower in the cytoplasmic and nuclear compartments compared with control cells. These results indicate that the drug does not prevent the phosphorylation of ERK1/2 by MEK1/2, but it does inhibit ERK1/2 protein kinase activity.

Germann et al. found that ulixertinib had antitumor activity in several xenograft studies including human $BRAF^{V600E}$-mutant lines (A375 melanoma, Colo205 colorectal) and $KRAS^{G12C}$-mutant MIAPACa-2 pancreatic cancer cells [127]. These investigators examined the antiproliferative effects of combining ulixertinib with the B-Raf inhibitors vemurafenib or dabrafenib in the $BRAF^{V600E}$-mutant melanoma cell lines G-361 and A375. They found that ulixertinib, vemurafenib, and dabrafenib were each active and they observed a modest synergy with a combination of ulixertinib with either B-Raf inhibitor. The synergy of ulixertinib combined with these B-Raf inhibitors in melanoma cell lines carrying a $BRAF^{V600E}$ mutation may translate into better clinical outcomes. Based upon studies with $BRAF^{V600E}$-mutant A375 cells, they found that resistance to ulixertinib was delayed when compared with the B-Raf inhibitor dabrafenib or the MEK1/2 inhibitor trametinib.

Secondary KRAS mutations are known drivers of resistance to MAP kinase pathway inhibitors [127]. To understand the susceptibility of ulixertinib to this mechanism of resistance, Germann et al. [127] studied an isogenic panel of clinically relevant KRAS mutations in the SW48 colorectal cell line. While several mutant KRAS alleles conferred resistance to MEK inhibition by trametinib or selumetinib, the sensitivity to ulixertinib was unaltered in the majority of these mutants; where a shift in sensitivity to ulixertinib was observed, it was not to the extent seen with trametinib or selumetinib. Overall, these results demonstrate that ulixertinib is more efficacious than MEK inhibitors in the context of *KRAS* mutations. The FDA-approved B-Raf (cobimetinib, dabrafenib, vemurafenib) and MEK (binimetinib, cobimetinib, trametinib) inhibitors are ineffective in the treatment of malignancies with *RAS* mutations. This emphasizes the need for inhibitors such as ulixertinib that are effective against tumors with *RAS* mutations. It remains to be established whether the ulixertinib findings translate into clinical effectiveness.

Sullivan et al. reported on a phase I ulixertinib dose-escalation clinical trial in patients with advanced solid tumors [128]. The study included patients with *BRAF* mutated colorectal cancers, melanomas, NSCLC, and other solid tumors as well as *NRAS*-mutated melanomas, and *MEK*-mutated solid tumors. They reported that partial responses were observed in 14% of patients. These responses were seen in patients with *NRAS, BRAF*^{600}, and non-*BRAF*^{600} tumors; the currently approved B-Raf inhibitors are not effective in the treatment of the latter category of cancers. These investigators reported that the adverse events included diarrhea, fatigue, nausea, and skin rashes. They also found that near complete inhibition (86%) of ERK activity in whole-blood samples in patients receiving the recommended dose of 600 mg twice daily. Of the several ERK inhibitors that have been studied, ulixertinib appears to be one of the more promising therapeutic agents.

The X-ray crystal structure of ulixertinib bound to ERK2 shows that a hydrogen bond forms between pyridine *N*1 and the N–H group of M108 and a second hydrogen bond forms between the drug amino group and the carbonyl oxygen of this third hinge residue. A polar bond forms between the drug carboxamide oxygen and the ε-amino group of K54 within the β3-strand and another polar bond forms between the hydroxyethyl group of the drug and the DFG-D167 carboxylate group (Fig. 6A). Ulixertinib makes numerous hydrophobic contacts with the enzyme including interactions with the β1-strand I31, E33 and Y36 within the glycine-rich loop, M38 and V39 (Cs7) within the β2-strand, A52 (CS8) and K54 of the AxK signature, I84 within the αC-β4 back loop, the Q85 gatekeeper residue (Sh2), D106 and L107 (the first two hinge residues), E109 and T110 before the αD-strand, K114 within the αD-strand, L156 (CS6), and C166, which is the x residue of xDFG. The 3-chloro group attached to the phenyl ring makes a halogen bond [125]

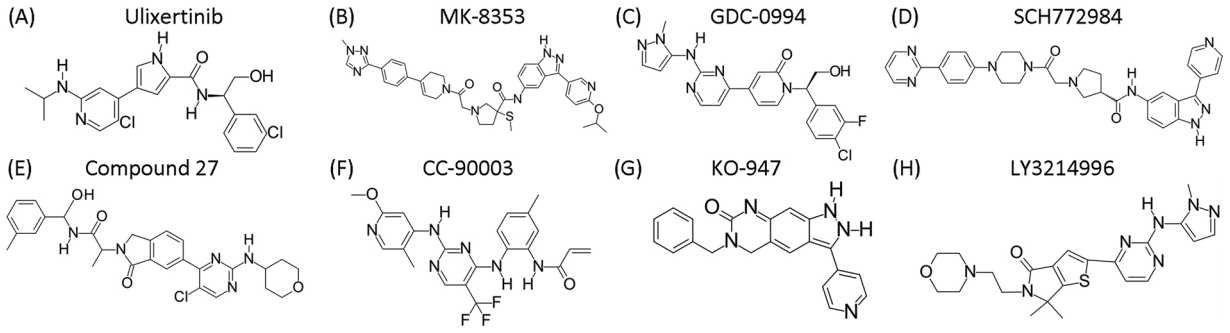

Fig. 5. Structures of selected ERK inhibitors that are in clinical trials.

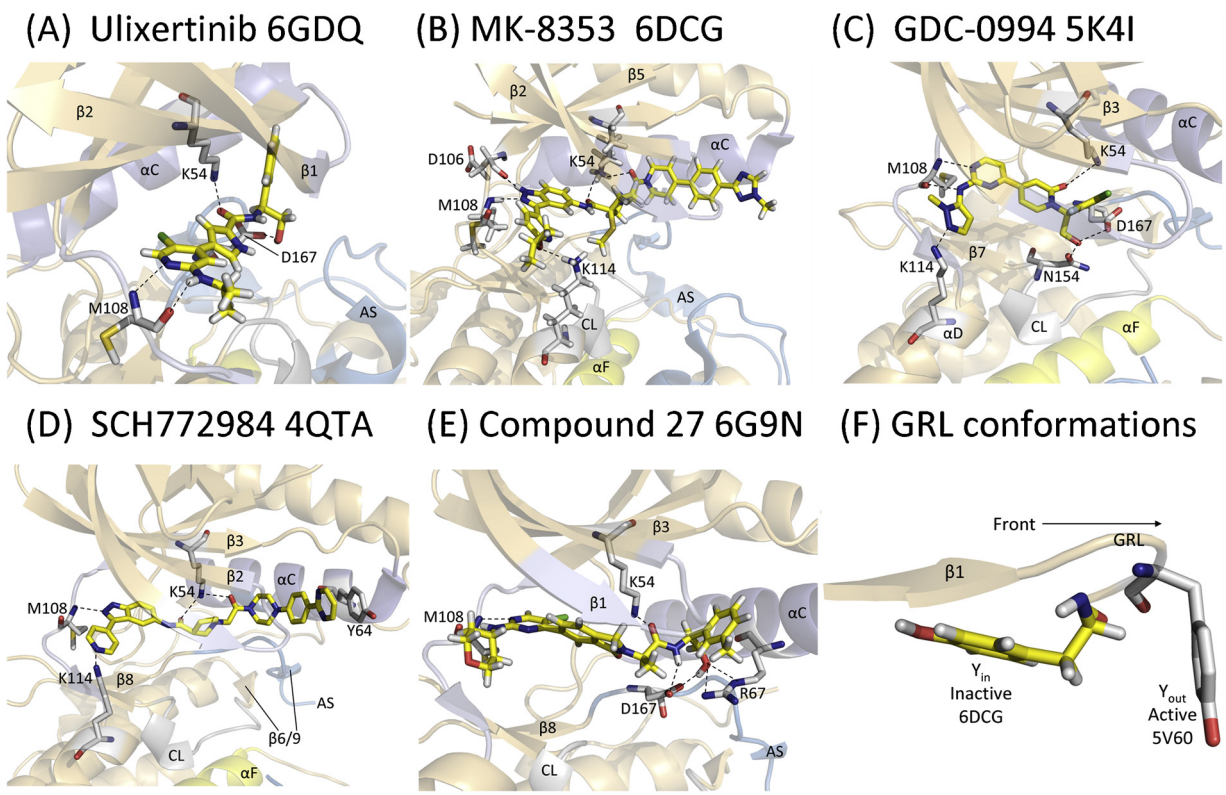

Fig. 6. (A–E). Structures of ERK2–drug complexes. The PDB IDs are given in the title. The carbon atoms of the drugs are colored yellow. AS, activation segment; CL, catalytic loop. The dashed lines depict polar bonds. (F) Side view of the superposition of the glycine-rich loops (GRL) of inactive rat (Y_{in}) and active human ERK2 (Y_{out}) with their respective PDB IDs.

with the glutamine gatekeeper residue and the 3-chloro group attached to the pyridine makes a halogen bond with Y36 of the glycine-rich loop. The drug occupies the front pocket and FP-II and it binds to an active form of ERK2 and is classified was a type I inhibitor [85]

MK-8353 is an indazole-pyrrolidine derivative that is under early clinical evaluation for the treatment of advanced/metastatic solid tumors (Fig. 5B). Boga et al. reported that this drug is a selective and potent inhibitor or ERK1/2 with IC_{50} values of 20/7 nM, respectively [129]. These investigators showed that the drug produced a concentration-dependent decrease in both pERK and pRSK in human A2058 $BRAF^{V600E}$-mutant melanoma cells in culture. The latter observation was unexpected because MK-8353 does not inhibit MEK1/2. The decrease in pRSK is a result of ERK inhibition and the decrease in pERK is apparently related to the inability of MEK to catalyze the phosphorylation of the ERK–MK-8353 complex; these characterize the ERK dual mechanism inhibition paradigm. MK-8353 exhibited antitumor activity of mice bearing human colon Colo205 xenografts. Moreover, MK-8353 exhibited good pharmacokinetic parameters in mouse, rat, dog, and monkey. Moschos et al. reported on the results of a phase I clinical trial of MK-8353 in patients with advanced solid tumors [130]. The toxicities to this agent were the same as those reported for the ulixertinib study. Skin biopsies from patients demonstrated decreased pERK levels. Patients with melanoma, colorectal cancer, pancreatic cancer, NSCLC, head and neck cancer, and papillary thyroid cancer were studied. Of 15 patients, partial responses were observed in three patients with melanoma. The authors stated that the use of combination therapies of MK-8353 and immunotherapies for select cancer types is under consideration.

The X-ray crystal structure shows that the indazole *N1* of MK-8353 makes a hydrogen bond with the backbone carbonyl group of D106 (the first hinge residue) and the indazole *N2* makes a hydrogen bond with the N–H group of M108 (the third hinge residue); the 2-propane oxypyridine oxygen forms a polar bond with the ε-amino group of K114 within the αD-helix. Moreover, the oxoethyl and the carboxamide oxygens form hydrogen bonds with ε-amino group of K54 of the β3-strand AxK signature (Fig. 6B). Although this result was obtained with the rat enzyme, the residue numbers correspond to those of the human enzyme. The drug makes numerous hydrophobic contacts with the enzyme. These include interactions with I31 of the β1-strand, A35 and Y36 in the glycine-rich loop, the β3-strand A52 (CS8), I56 and P58 in the β3-αC front loop in the ceiling of the drug binding site, Y64 and T68 in the αC-helix, I84 in the αC-β4 back loop, I103 near the end of the β5-strand, L107 (the second hinge residue), S153 and N154 within the catalytic loop, C166 (the x of xDFG), and DFG-D167 and DFG-F168 of the activation segment. The drug is found in the front pocket and gate area. The R-spine of ERK2 is broken between R2 and R3 with R3 displaced backward and Y36 of the catalytic loop occurs under the glycine-rich loop (not shown) precluding the binding of ATP. MK-8353 is thus a type I½B inhibitor that binds to an inactive DFG-D_{in} conformation [85].

GDC-0994 is a pyrazole amino-pyrimidine derivative (Fig. 5C) that is under early clinical evaluation for the treatment of advanced/metastatic solid tumors as monotherapy or in combination with cobimetanib. Blake et al. reported that the drug is a selective and potent inhibitor of ERK1/2 with IC_{50} values of 6.1/3.1 nM, respectively [131]. They performed studies with nude mice bearing human *KRAS* colorectal tumor implants and they found significant tumor growth inhibition and decreased phosphorylation of RSK. They studied its pharmacokinetic parameters in rat, mouse, dog, and cynomolgus monkey. Phase I dose-escalation clinical trials are underway with oral GDC-0994 given once daily using a 21-day on and 7-day off protocol. Additional studies will be required to establish the clinical efficacy of this prospective therapeutic agent.

The X-ray crystal structure shows that the pyrazole *N2* of GDC-0994 forms a hydrogen bond with the ε-amino group of K114 within the αD-helix; the amino group of the drug forms a hydrogen bond with the carbonyl group of M108 and the pyrimidine *N1* forms a hydrogen bond

with the N–H group of this third hinge residue (Fig. 6C). The pyridine-2-one oxygen forms a hydrogen bond with the ε-amino group of K54 of the AxK signature and the hydroxyethyl alcohol forms polar bonds with the oxygen atoms of the R-groups of catalytic loop N154 and DFG-D167. The drug makes hydrophobic contact with I31 of the β1-strand, M38 and V39 (CS7) in the β2-strand, A52 (CS8) and K54 of the AxK signature, the Q105 gatekeeper (Sh2), L107 and T110 of the hinge, the catalytic loop N154, L156 (CS6), and C166 (the x residue of xDFG) as well as DFG-D167. The 4-chloro atom attached to the phenyl ring makes a halogen bond with M38 of the glycine-rich loop and the adjacent 3-fluoro atom makes van der Waals contact with V39 (CS7) of the β2-strand. GDC-0994 is located in the front pocket and gate area. It binds to an active form of ERK2 and is classified as a type I inhibitor [85].

SCH772984, which is an indazole-pyrrolidine derivative (Fig. 5D) like MK-8353, is a selective ERK1/2 inhibitor [132,133]. Morris et al. developed this compound and found that the IC_{50} values for ERK1/2 were 4/1 nM, respectively [132]. They also found that the drug inhibited the phosphorylation of RSK (an ERK substrate) and ERK itself in the *BRAF*^{V600E}-mutant human melanoma cell line LOXIMV1 (LOX). This represents another example of the dual ERK mechanism of inhibition. The drug possessed antitumor activity against various cell *BRAF, KRAS,* and *NRAS* mutant colorectal, melanoma, and pancreatic cell lines and their xenograft counterparts. These investigators found that SCH772984 is effective against cells with clinically relevant BRAF or MEK inhibitor resistance mechanisms including (i) overexpression of *BRAF*^{V600E}, (ii) a B-Raf splice-variant lacking an amino-terminal RAS-binding domain, (iii) acquired *RAS* mutations, (iv) acquired *MEK1* mutations as well as (v) ectopic expression of various *MEK1* mutants.

The X-ray crystal structure of SCH772984 bound to human ERK2 shows that a hydrogen bond forms between K114 $-NH_3^+$ of the αD-helix and the *N1* of the pyridine moiety; another hydrogen bond forms between the *N2* indazole and the N–H group of M108 (the third hinge residue) and the ε-amino group of K54 of the AxK signature forms polar bonds with each of the two carbonyl oxygens of the drug (Fig. 6D). SCH772984 makes hydrophobic contacts with I31 of the β1-strand, A35 and Y36 of the glycine-rich loop, V39 (CS7) of the β2-strand, A52 (CS8) and K54 of the AxK signature, I56 in the β3-strand, R67, T68, and E71 of the αC-helix, I84 in the back loop, the gatekeeper Q105 as well as L107, E109, T110, D111 of the hinge, L156 (CS6), C166 (the x of xDFG), and DFG-D167. Although the drug abuts the αC-helix, it is far from the αE-helix and is not in the back cleft; it occurs in the front pocket and gate area of the enzyme. The interaction of the drug with Y36 of the glycine-rich loop is unusual in that the R-group occurs underneath the loop (the glycine-rich loop "in" conformation) while in active enzymes it occurs out of the loop (Fig. 6F). Owing to its "in" location, the enzyme is inactive because Y36 sterically precludes the binding of ATP. Accordingly, SCH772984 is a type I½B inhibitor (an inactive structure with DFG-D_{in}) [85]. It is unclear whether the drug will enter clinical trials.

Compound **27** is an aminopyrimidine isoindolinone that is under development by Astex Pharmaceuticals (Fig. 5E). Heightman et al. described the formulation of this ligand by a fragment-based discovery protocol [133]. They found that the IC_{50} value for the drug against ERK2 was 3 nM. Moreover, the IC_{50} values for the inhibition of the growth of human *BRAF*^{V600E} mutant A375 melanoma cells and Colo205 colon cancer cells were 4.9 nM and 7.5 nM, respectively. The drug also inhibited the growth of xenografts of the Colo205 cells. Compound **27** inhibited the phosphorylation of the ERK substrate RSK as well as the phosphorylation of ERK itself. Accordingly, it appears to be an ERK dual mechanism inhibitor.

The X-ray crystal structure of compound **27** bound to human ERK2 shows that the *N*1 of the pyrimidine moiety forms a hydrogen bond with the N–H group of third hinge residue (M108) and the drug carbonyl group forms a hydrogen bond with the ε-amino group of the β3-strand K54. Furthermore, the amide N–H group and the hydroxyethyl group of the drug each forms a hydrogen bond with the carboxylate group of DFG-D167 and the hydroxyethyl oxygen forms polar bonds with guanidinium nitrogens of R67 within the αC-helix (Fig. 6E). The drug makes hydrophobic contacts with I31 of the β1-strand, A35 and Y36 of the glycine-rich loop, V39 (CS7) of the β2-strand, A52 (CS8) and K54 of the AxK signature, I56 and P58 in the β3-strand, Y64, R67, T68, and E71 of the αC-helix, I84 in the back loop, the gatekeeper Q105 as well as L107, E109, T110, D111 of the hinge, L156 (CS6), C166 (the x of xDFG), DFG-D167, and L170 within the activation segment. Y36 within the glycine-rich loop is found beneath the loop as described above for SCH772984. The drug occurs within the front pocket, FP-II, and the gate area. The drug is a type I½B inhibitor because it binds to an inactive enzyme with an inactive glycine-rich loop conformation, DFG-D_{in}, and it does not extend past the gatekeeper residue [85]. It is unclear whether the drug will enter clinical trials.

Fig. 5F–H depict the structures of three ERK antagonists: CC-90003, KO-947, and LY3214996 [134,135]. These drugs are in clinical trials as monotherapies or combination therapies for various advanced/metastatic tumors. Unfortunately, we lack X-ray crystal structures of these drugs bound to any protein kinase. Table 4 lists three additional ERK antagonists that are in clinical trials (LTT-462, LY3214006, ONC201), the structures of which are not publicly available. See Refs. [57,136] for information on additional ERK antagonists that are research tools or that are or were in preclinical or clinical phases of study. These include AEZS-131, AEZS-136, BL-EI-001, FR180204, FR148083, VTX-11e, and AZ13767370.

As observed with all MAP kinase pathway inhibitors, treatment with ERK inhibitors is likely to cause resistance. Jaiswal et al. tested five structurally different ATP-competitive ERK inhibitors including GDC-0994 and SCH772984 on *BRAF/RAS*-mutant cancer cell lines of different tissue types to generate resistant lines [137]. They used genomic analysis and structural biology to discover the mechanisms leading ERK1/2-inhibitor resistance. They identified *ERK1/2* mutations, amplification and overexpression of ERK2 as well as overexpression of EGFR and ErbB2 as mechanisms of acquired resistance. Structural analyses showed that the drugs exhibited impaired ability to bind to mutant ERK molecules. Besides MEK inhibitors, ErbB receptor and PI3K/mTOR pathway inhibitors were effective in overcoming ERK-inhibitor resistance. These authors suggested that combination therapy of MEK, ErbB receptor, or PI3K/mTOR inhibitors with ERK inhibitors may be an effective strategy for managing the emergence of resistance in patients.

7. Physicochemical properties of selected ERK inhibitors

7.1. Lipinski's rule of five

Medicinal chemists and pharmacologists have searched for drug-like chemical properties that result in compounds with oral therapeutic efficacy in a predictable fashion. Lipinski's rule represents a computational and experimental approach to estimate permeability, solubility, and efficacy in the drug discovery and development setting [138]. In the drug development process the "rule of 5″ predicts that poor permeation or absorption is more likely when there are more than 5 hydrogen-bond donors, 10 (5 × 2) hydrogen-bond acceptors, a molecular weight greater than 500 (5 × 100) and a calculated Log P (cLogP) greater than 5. P represents the partition coefficient and it is the ratio of the solubility of the un-ionized drug in water saturated with 1-octanol divided by the solubility of the un-ionized drug in 1-octanol saturated with water; the greater the P value, the greater the hydrophobicity. The number of hydrogen-bond donors is expressed as the sum of OH and NH groups and the number of hydrogen-bond acceptors is taken as any heteroatom without a formal positive charge with the exception of heteroaromatic oxygen and sulfur, pyrrole nitrogen, halogens, and higher oxidation states of nitrogen, phosphorus, and sulfur but including the oxygens bonded to them. The empirical rule of 5 was based

on the chemical properties of more than two thousand drugs [138]. Of the eight selected ERK inhibitors with known chemical and biological properties (Table 4), three (MK-8353, SCH772984, and compound **27**) have molecular weights greater than 500. Otherwise, these selected drugs have properties consistent with the rule of five.

7.2. The importance of lipophilicity

7.2.1. Lipophilic efficiency, LipE

Since the publication of the rule of five in 1997 [138], additional studies of the physicochemical contributions to drug-likeness have led to various refinements [139–146]. The concept of lipophilic efficiency, or LipE, is a useful test of the tendency to use lipophilicity-driven binding as a strategy to increase potency. The formula for calculating lipophilic efficiency is given by the following equations:

$$\text{LipE} = \text{p}IC_{50} - \text{cLogD} \text{ or } \text{LipE} = \text{p}K_i - \text{cLogD}$$

Similar to its usage in expressing the hydrogen ion concentration as pH, the p is an operator that represents the negative of the Log_{10} of the IC_{50} or the or the negative of Log_{10} of the K_i. cLogD is the calculated log of the Distribution coefficient, which is the ratio of the drug solubility (both ionized and un-ionized) in 1-octanol and water in a mixture of immiscible 1-octanol/water at a specified pH, usually 7.4.

The second term (– cLogD or minus cLogD) represents the lipophilicity of a compound or drug where c indicates that the value is calculated, or computed, using an algorithm based upon the behavior of thousands of organic compounds. The more soluble the compound is in 1-octanol in an immiscible 1-octanol/water mixture, the greater is its lipophilicity and the greater is the value of – cLogD. Leeson and Springthorpe suggest that compound lipophilicity, as estimated by – cLogP, is the most important chemical property to consider during drug development [141]. Their use of – cLogP was based upon results obtained prior to the use of D, the distribution coefficient. For practical purposes, $cLog_{10}P$ or $cLog_{10}D$ can be used interchangeably to compare a series of compounds. Lipophilicity plays an important role in promoting binding to unwanted drug targets. The goal for drug optimization during development is to increase inhibitory power without simultaneously increasing lipophilicity. LipE is an approximate guide to specificity and facilitates lead optimization by permitting a comparison of drug congeners based upon the use of the same assay to make comparisons valid [145].

cLogD can be determined for several compounds by computer in a matter of minutes; the experimental determination of LogD is labor intensive and is performed only in select cases. Proposed optimal values of LipE range from 5 to 10 [140]. Increasing potency and decreasing the lipophilicity during drug development, in general, lead to better pharmacological properties. The values of LipE calculated on the basis of biochemical K_i or IC_{50} values for selected ERK inhibitors are given in Table 4. Of the five drugs with calculated LipE values, only MK-8353 falls out of the proposed optimal range.

7.2.2. Ligand efficiency, LE

The ligand efficiency (LE), which is another useful molecular property, is a measurement that relates the potency per heavy atom (non-hydrogen atom) of a drug. The LE is given by the following equation:

$$\text{LE} = \Delta G^{\circ\prime}/\text{N} = -\text{RTln}K_{eq}/\text{N} = -2.303\text{RTLog}_{10}K_{eq}/\text{N}$$

$\Delta G^{\circ\prime}$ represents the standard free energy change of the drug binding to its target at pH 7, N is the number of non-hydrogen atoms (heavy atoms) in the drug, R is the universal temperature-energy coefficient, or gas constant (0.00198 kcal/degree-mole), T is the temperature in degrees Kelvin, and K_{eq} is the equilibrium constant. Proposed optimal values of LE are greater than 0.3 kcal/mol. The K_i or IC_{50} values are used as a surrogate of the equilibrium constant. At 37 °C, or 310 K, this equation becomes $-(2.303 \times (0.00198\ \text{kcal/mol-K}) \times 310\ \text{K}\ Log_{10}K_{eq})/\text{N}$ or $-1.41\ Log_{10}K_{eq}/\text{N}$. LE was first proposed as a method for comparing drugs according to their average binding energy per atom. This parameter is used in the selection of lead compounds and is particularly useful in fragment-based drug discovery [145].

The ligand efficiency represents the relative binding affinity per non-hydrogen atom of the drug or ligand of interest. The value of N serves as a substitute for the molecular weight. LE is inversely proportional to the value of N and is directly proportional to the binding affinity and $-Log_{10}K_{eq}$. The values of LE calculated in the basis of biochemical K_i or IC_{50} values for selected ERK inhibitors are provided in Table 4. The LE values of ulixertinib, revoxertinib, and compound **27** fall into a satisfactory range and are greater than 0.3. The values for lipophilic efficiency (LipE) and ligand efficiency (LE) listed in Table 4 were calculated from experiments performed under a variety of different conditions. Accordingly, LipE and LE values alone cannot be used to make a direct comparison of the drugs because of differences in methodology. The examples were derived from various drug discovery efforts and are meant to provide representative values.

8. Epilogue and perspective

At the end of 2018, the US FDA had approved 48 small molecule protein kinase inhibitors (see supplementary material), nearly all of which are orally effective with the exception of temsirolimus (which is given intravenously) and netarsudil (which is given as an eye drop). Of the 48 approved small molecule protein kinase inhibitors, the majority (25) inhibit receptor protein-tyrosine kinases, 10 inhibit non-receptor protein-tyrosine kinases, and 13 are directed at protein-serine/threonine protein kinases including the dual specificity protein kinases MEK1/2. A total of 43 are directed toward malignancies (36 against solid tumors including lymphomas and 7 against non-solid tumors, e.g., leukemias). At least 18 of the approved drugs are multikinase inhibitors. This has advantages and disadvantages. It may be that the therapeutic effectiveness of these drugs may be related to the inhibition of more than one enzyme. For example, cabozantinib and sunitinib have potent AXL off-target activity, which may add to their clinical effectiveness [147]. On the other hand, the inhibition of non-target enzymes may lead to various toxicities. Accordingly, we have the question of whether magic shotguns are to be favored over magic bullets [148].

A total of seven drugs are directed toward non-malignancies; baricitinib and tofacitinib are used in the treatment of rheumatoid arthritis, fostamatinib is used for the treatment of chronic immune thrombocytopenia, nintedanib is used in the treatment of idiopathic pulmonary fibrosis, ruxolitinib is used for the treatment of myelofibrosis and polycythemia vera, sirolimus is used to prevent rejections following renal transplantation, and netarsudil is used to treat glaucoma (See supplemental material) [149]. Six drugs inhibit their target enzyme covalently including acalabrutinib (targeting BTK in mantle cell lymphoma), afatinib (targeting EGFR in NSCLC), dacomitinib (targeting mutant *EGFR* in lung cancer), neratinib (targeting ErbB2 in HER2-positive lung cancer), ibrutinib (targeting BTK in mantle cell lymphomas, chronic lymphocytic leukemia, marginal zone lymphomas, chronic graft vs. host disease, and Waldenström macroglobulinemia), and osimertinib (targeting *EGFR* T970 M mutants in NSCLC). Imatinib is a broad-spectrum disease inhibitor; it is approved for the treatment of eight disorders including Philadelphia chromosome-positive chronic myelogenous leukemia, Philadelphia chromosome-positive acute lymphoblastic leukemia, aggressive systemic mastocytosis, chronic eosinophilia leukemia, hypereosinophilic syndrome, dermatofibrosarcoma protuberans, gastrointestinal stromal tumors, and myelodysplastic/myeloproliferative diseases.

Larotrectinib was the first tissue-agnostic protein kinase inhibitor approved by the US FDA (2018) for the treatment of adult and pediatric solid tumors that have a neurotrophic receptor kinase (*NTRK*) gene

fusion protein; it is called tissue agnostic because it is used for the treatment of any cancer bearing the fusion protein irrespective of the anatomical location. The first tissue-agnostic drug approved by the FDA (2017) was pembrolizumab; it blocks the programed cell death receptor (PD-1) of lymphocytes and is used in the treatment of patients with unresectable or metastatic microsatellite instability-high (MSI-H) or mismatch repair deficient (dMMR) solid tumors. Pembrolizumab is also approved for the treatment of NSCLC and head and neck squamous cell carcinomas, which are anatomically based malignancies, as well as melanomas and Hodgkin lymphomas.

Manning et al. reported that the human protein kinase super family consists of 518 members [2]. Because mutations and dysregulation of protein kinases play fundamental roles in the pathogenesis of many human diseases, this family of enzymes has become one of the most important drug targets over the past several decades [150]. There are four dozen FDA-approved medications that are directed against about 20 different protein kinases (www.brimr.org/PKI/PKIs.htm). Moreover, there are about 200 drugs in clinical trials worldwide that are directed against another two dozen protein kinases (http://www.icoa.fr/pkidb/) [42]. Owing to the 244 disease loci and cancer amplicons that have been mapped in the human genome [2], it is likely that there will be a significant increase in the number of enzymes that will be studied for the treatment of many more illnesses. Several possibilities are listed in Table 5.

Although the pose or mode of binding of each drug with its target protein kinase is unique, it is helpful to classify drug-enzyme interactions for their use in drug discovery and development protocols. We have previously classified protein kinase antagonists into seven conceivable types (I–VI and I½) that are based upon the nature of the drug-protein kinase complexes [85]. The complexity of inhibitor taxonomy increases because some agents bind to different conformations of their protein kinase targets. For example, bosutinib is a type IIB inhibitor of Abl and a type I inhibitor of Src (both are non-receptor protein-tyrosine kinases). Furthermore, crizotinib is a type I½B antagonist of c-Met and a type I inhibitor of ALK (both are receptor protein-tyrosine kinases). Sunitinib is a type IIB inhibitor of Kit (a receptor protein-tyrosine kinase) and a type I½B inhibitor of CDK2 (a protein-serine/threonine kinase). Adding to this intricacy, X-ray crystallographic structures demonstrate that erlotinib can be a type I or I½B inhibitor of EGFR/ErbB1 (a receptor protein-tyrosine kinase). These results indicate that some protein kinase inhibitors lack conformational selectivity. Adding to the complexity are studies with imatinib, which is the prototypical type IIA DFG-D_{out} inhibitor, that show that it binds to the active non-receptor Syk (spleen tyrosine kinase) making it also a type I inhibitor (PDB ID: 1XBB). In addition to binding as a type II antagonist in a linear extended conformation, imatinib adopts a compact U-shaped structure as a type I Syk antagonist and binds only within the front pocket. Different modes of binding are related to ligand conformational flexibility and the number of rotatable bonds possessed by the ligand.

The Ras-Raf-MEK-ERK MAP kinase signal transduction module is one of the most prevalent oncogenic pathways in human cancers [8–12,163]. *RAS* mutations occur in a wide variety of cancers including 70% of pancreatic ductal adenocarcinomas, 40% of colorectal cancers, and 35% of non-small cell lung cancers (NSCLC). Tumors that are driven with *BRAF* mutations include 90% of skin melanomas, 10–70% of thyroid cancers (depending upon the histology), about 10% of colorectal cancers, and 4% of NSCLC [37–41]. Although numerous cancers are driven by the activation of the MAP kinase pathway, thus far the only approved drugs that block this pathway are used for the treatment of *BRAF*-mutant melanomas (www.brimr.org/PKI/PKIs.htm). The best treatments include the combination of B-Raf with a MEK inhibitor (dabrafenib and trametinib, encorafenib and binimetinib, vemurafenib and cobimetanib). Owing to the large variety of malignancies that are driven by dysregulation of the MAP kinase pathway, additional tumor types should be amenable to MAP kinase pathway inhibitor therapy. Besides new B-Raf and MEK inhibitors, the addition of ERK inhibitors should prove helpful. The use of Ras inhibitors should also be efficacious; owing to the undruggable nature of Ras because it lacks a reasonable drug binding cavity, it may take a much longer time to implement this strategy.

The role of regulatory protein phosphorylation in tumorigenesis began in the Ben May Laboratory for Cancer Research at the University of Chicago in the 1950s. Williams-Ashman and Kennedy discovered that protein phosphorylation was very active in Ehrlich ascites tumor cells [164]. Subsequently, Kennedy and Smith isolated radioactive phosphoserine from the protein fraction of these tumor cells after incubation with [^{32}P]-phosphate [165]. These investigators demonstrated that the phosphoserine phosphate in the protein fraction rapidly turns over. Although the significance of this rapid turnover was unknown at the time, they wrote presciently that such turnover “suggests a function of some importance.” In 1954, Burnett and Kennedy were the first to characterize protein kinase enzyme activity [166]. They used rat liver as the source of their enzyme and found that bovine serum albumin, γ-globulin, lysozyme, and ovalbumin failed to serve as substrates whereas casein was readily phosphorylated. They isolated and identified [^{32}P]-phosphoserine following acid hydrolysis of the casein product. Moreover, they demonstrated that Mg^{2+} and ATP were required for protein kinase enzyme activity. This was the only paper that these authors published on protein kinases leaving later work to other investigators.

The MAP kinase pathway is an important evolutionarily conserved signaling module that is stringently regulated by (i) numerous activation processes and by (ii) short-term and long-term negative feedback inhibition [19]. Perhaps it should be expected that any perturbation by a pathway inhibitor would be countered with pathway re-activation by

Table 5
Novel protein kinase targets and diseases.

Target	Diseases
SPAK/OSR1	Hypertension [150]
Rho, Rho kinase	Cardiovascular disease (hypertension, cerebral vasospasm, coronary vasospasm, myocardial infarction and heart failure) [151]
P38α Map kinase	Asthma, atherosclerosis, Crohn disease, psoriasis, and rheumatoid arthritis [152]
JAK1/2	Lupus erythematosus [153]
RET	Irritable bowel syndrome [154]
Trk	Pain [155]
LRRK2	Parkinson disease [150]
Glycogen synthase kinase-3β	Parkinson disease [156]
TTBK1	Neurodegenerative diseases (Alzheimer disease, amyotrophic lateral sclerosis, and spinocerebellar ataxia type 11) [157]
Fyn	Alzheimer disease [158]
DLK (MAP3K12)	Alzheimer disease [159]
Glycogen synthase kinase-3β	Amyotrophic lateral sclerosis [160]
SRPK1	Wet age-related macular degeneration [161]
PDGFR	Wet age-related macular degeneration [161,162]
VEGFR	Wet age-related macular degeneration [161,162]

servomechanisms. Thus, despite the effectiveness of the combination of a B-Raf and MEK inhibitor in the treatment of melanomas, resistance to such treatments occurs in about one year. Assuming that effective ERK inhibitors can be developed, it remains to be seen whether these inhibitors will be effective against Raf/MEK inhibitor-therapy resistant tumors. If so, additional studies will be required to determine the best strategy for the administering these drugs. Should the Raf-MEK inhibitors be given until resistance occurs, should Raf-MEK-ERK inhibitors be given together, or should ERK inhibitors be given first? Another possibility to prevent or forestall the development of resistance to targeted inhibitors is to simultaneously block pathways parallel to the MAP kinase pathway such as the PI-3 kinase AKT/PKB pathway [167]. Despite the success in the use of protein kinase inhibitor therapies in the treatment of various cancers, the universal development of drug resistance is a vexing problem that can only be solved with additional experimentation.

Conflict of interest

The author is unaware of any affiliations, memberships, or financial holdings that might be perceived as affecting the objectivity of this review.

Acknowledgments

The author thanks Laura M. Roskoski for providing editorial and bibliographic assistance. I also thank Josie Rudnicki and Jasper Martinsek help in preparing the figures and Pasha Brezina and W.S. Sheppard for their help in structural analyses. The colored figures in this paper were evaluated to ensure that their perception was accurately conveyed to colorblind readers [168].

Appendix A. Supplementary data

Supplementary material related to this article can be found, in the online version, at doi:https://doi.org/10.1016/j.phrs.2019.01.039.

References

[1] T. Hunter, Signaling–2000 and beyond, Cell 100 (2000) 113–127.
[2] G. Manning, D.B. Whyte, R. Martinez, T. Hunter, S. Sudarsanam, The protein kinase complement of the human genome, Science 298 (2002) 1912–1934.
[3] A. Alonso, J. Sasin, N. Bottini, I. Friedberg, I. Friedberg, A. Osterman, et al., Protein tyrosine phosphatases in the human genome, Cell 117 (2004) 699–711.
[4] A. Burgess, J. Vuong, S. Rogers, M. Malumbres, S.I. O'Donoghue, SnapShot: phosphoregulation of mitosis, Cell 169 (2017) 1358–1358.e1.
[5] A. Bononi, C. Agnoletto, E. De Marchi, S. Marchi, S. Patergnani, M. Bonora, et al., Protein kinases and phosphatases in the control of cell fate, Enzyme Res. (2011), https://doi.org/10.4061/2011/329098.
[6] H.J. Schaeffer, M.J. Weber, Mitogen-activated protein kinases: specific messages from ubiquitous messengers, Mol. Cell. Biol. 19 (1999) 2435–2444.
[7] A.S. Dhillon, S. Hagan, O. Rath, W. Kolch, MAP kinase signalling pathways in cancer, Oncogene 26 (2007) 3279–3290.
[8] M. Cargnello, P.P. Roux, Activation and function of the MAPKs and their substrates, the MAPK-activated protein kinases, Microbiol. Mol. Biol. Rev. 75 (2011) 50–83.
[9] A. Plotnikov, E. Zehorai, S. Procaccia, R. Seger, The MAPK cascades: signaling components, nuclear roles and mechanisms of nuclear translocation, Biochim. Biophys. Acta 1813 (2011) 1619–1633.
[10] D.K. Morrison, R.J. Davis, Regulation of MAP kinase signaling modules by scaffold proteins in mammals, Annu. Rev. Cell Dev. Biol. 19 (2003) 91–118.
[11] A.J. Whitmarsh, The JIP family of MAPK scaffold proteins, Biochem. Soc. Trans. 34 (2006) 828–832.
[12] R. Roskoski Jr, Targeting oncogenic Raf protein-serine/threonine kinases in human cancers, Pharmacol. Res. 135 (2018) 239–258.
[13] M. Malumbres, M. Barbacid, RAS oncogenes: the first 30 years, Nat. Rev. Cancer 3 (2003) 459–465.
[14] A.G. Stephen, D. Esposito, R.K. Bagni, F. McCormick, Dragging Ras back in the ring, Cancer Cell 25 (2014) 272–281.
[15] D.K. Simanshu, D.V. Nissley, F. McCormick, RAS proteins and their regulators in human disease, Cell 170 (2017) 17–33.
[16] R. Roskoski Jr, RAF protein-serine/threonine kinases: structure and regulation, Biochem. Biophys. Res. Commun. 399 (2010) 313–317.
[17] R. Roskoski Jr, MEK1/2 dual-specificity protein kinases: structure and regulation, Biochem. Biophys. Res. Commun. 417 (2012) 5–10.
[18] R. Roskoski Jr, Allosteric MEK1/2 inhibitors including cobimetanib and trametinib in the treatment of cutaneous melanomas, Pharmacol. Res. 117 (2017) 20–31.
[19] R. Roskoski Jr, ERK1/2 MAP kinases: structure, function, and regulation, Pharmacol. Res. 66 (2012) 105–143.
[20] E.B. Ünal, F. Uhlitz, N. Blüthgen, A compendium of ERK targets, FEBS Lett. 591 (2017) 2607–2615.
[21] M. Raman, W. Chen, M.H. Cobb, Differential regulation and properties of MAPKs, Oncogene 26 (2007) 3100–3112.
[22] C.R. Weston, R.J. Davis, The JNK signal transduction pathway, Curr. Opin. Cell Biol. 19 (2007) 142–149.
[23] S.K. Hanks, Eukaryotic protein kinases, Curr. Opin. Struct. Biol. 1 (1991) 369–383.
[24] R. Lefloch, J. Pouysségur, P. Lenormand, Total ERK1/2 activity regulates cell proliferation, Cell Cycle 8 (2009) 705–711.
[25] A.A. Samatar, P.I. Poulikakos, Targeting RAS-ERK signalling in cancer: promises and challenges, Nat. Rev. Drug Discov. 13 (2014) 928–942.
[26] S. Faivre, S. Djelloul, E. Raymond, New paradigms in anticancer therapy: targeting multiple signaling pathways with kinase inhibitors, Semin. Oncol. 33 (2006) 407–420.
[27] A.T. Baines, D. Xu, C.J. Der, Inhibition of Ras for cancer treatment: the search continues, Future Med. Chem. 3 (2011) 1787–1808.
[28] A.Q. Khan, S. Kuttikrishnan, K.S. Siveen, K.S. Prabhu, M. Shanmugakonar, H.A. Al-Naemi, et al., RAS-mediated oncogenic signaling pathways in human malignancies, Semin. Cancer Biol. (2018) pii: S1044-579X(18)30002–6.
[29] Y. Pylayeva-Gupta, E. Grabocka, D. Bar-Sagi, RAS oncogenes: weaving a tumorigenic web, Nat. Rev. Cancer 11 (2011) 761–774.
[30] J.M. Ostrem, K.M. Shokat, Direct small-molecule inhibitors of KRAS: from structural insights to mechanism-based design, Nat. Rev. Drug Discov. 15 (2016) 771–785.
[31] A.V. Statsyuk, Let K-Ras activate its own inhibitor, Nat. Struct. Mol. Biol. 25 (2018) 435–437.
[32] R. Hansen, U. Peters, A. Babbar, Y. Chen, J. Feng, M.R. Janes, et al., The reactivity-driven biochemical mechanism of covalent $KRAS^{G12C}$ inhibitors, Nat. Struct. Mol. Biol. 25 (2018) 454–462.
[33] H.C. Chuang, P.H. Huang, S.K. Kulp, C.S. Chen, Pharmacological strategies to target oncogenic KRAS signaling in pancreatic cancer, Pharmacol. Res. 117 (2017) 370–376.
[34] J.P. O'Bryan, Pharmacological targeting of RAS: recent success with direct inhibitors, Pharmacol. Res. (2018), https://doi.org/10.1016/j.phrs.2018.10.021 pii: S1043-6618(18)31566-4.
[35] E. Hodis, I.R. Watson, G.V. Kryukov, S.T. Arold, M. Imielinski, J.P. Theurillat, et al., A landscape of driver mutations in melanoma, Cell 150 (2012) 251–263.
[36] Cancer Genome Atlas Network, Genomic classification of cutaneous melanoma, Cell 161 (2015) 1681–1696.
[37] H. Namba, M. Nakashima, T. Hayashi, N. Hayashida, S. Maeda, T.I. Rogounovitch, et al., Clinical implication of hot spot *BRAF* mutation, V599E, in papillary thyroid cancers, J. Clin. Endocrinol. Metab. 88 (2003) 4393–4397.
[38] J.C. Jones, L.A. Renfro, H.O. Al-Shamsi, A.B. Schrock, A. Rankin, B.Y. Zhang, et al., $^{Non\text{-}V600}$*BRAF* mutations define a clinically distinct molecular subtype of metastatic colorectal cancer, J. Clin. Oncol. 35 (2017) 2624–2630.
[39] S. Cardarella, A. Ogino, M. Nishino, M. Butaney, J. Shen, C. Lydon, et al., Clinical, pathologic, and biologic features associated with *BRAF* mutations in non-small cell lung cancer, Clin. Cancer Res. 19 (2013) 4532–4540.
[40] P.K. Paik, M.E. Arcila, M. Fara, C.S. Sima, V.A. Miller, M.G. Kris, et al., Clinical characteristics of patients with lung adenocarcinomas harboring *BRAF* mutations, J. Clin. Oncol. 29 (2011) 2046–2051.
[41] S.T. Yuen, H. Davies, T.L. Chan, J.W. Ho, G.R. Bignell, C. Cox, et al., Mutations of the *BRAF* gene in human cancer, Nature 417 (2002) 949–954.
[42] P.M. Fischer, Approved and experimental small-molecule oncology kinase inhibitor drugs: a mid-2016 overview, Med. Res. Rev. 37 (2017) 314–367.
[43] T. Eisen, T. Ahmad, K.T. Flaherty, M. Gore, S. Kaye, R. Marais, et al., Sorafenib in advanced melanoma: a Phase II randomised discontinuation trial analysis, Br. J. Cancer 95 (2006) 581–586.
[44] P.B. Chapman, A. Hauschild, C. Robert, J.B. Haanen, P. Ascierto, J. Larkin, et al., Improved survival with vemurafenib in melanoma with BRAF V600E mutation, N. Engl. J. Med. 364 (2011) 2507–2516.
[45] Y. Zhao, A.A. Adjei, The clinical development of MEK inhibitors, Nat. Rev. Clin. Oncol. 11 (2014) 385–400.
[46] A. Hauschild, J.J. Grob, L.V. Demidov, T. Jouary, R. Gutzmer, M. Millward, et al., Dabrafenib in *BRAF*-mutated metastatic melanoma: a multicentre, open-label, phase 3 randomised controlled trial, Lancet 380 (2012) 358–365.
[47] K.T. Flaherty, C. Robert, P. Hersey, P. Nathan, C. Garbe, M. Milhem, et al., Improved survival with MEK inhibition in BRAF-mutated melanoma, N. Engl. J. Med. 367 (2012) 107–114.
[48] K.B. Kim, R. Kefford, A.C. Pavlick, J.R. Infante, A. Ribas, J.A. Sosman, et al., Phase II study of the MEK1/MEK2 inhibitor trametinib in patients with metastatic *BRAF*-mutant cutaneous melanoma previously treated with or without a BRAF inhibitor, J. Clin. Oncol. 31 (2013) 482–489.
[49] K.T. Flaherty, J.R. Infante, A. Daud, R. Gonzalez, R.F. Kefford, J. Sosman, et al., Combined BRAF and MEK inhibition in melanoma with BRAF V600 mutations, N. Engl. J. Med. 367 (2012) 1694–1703.
[50] J. Larkin, P.A. Ascierto, B. Dréno, V. Atkinson, G. Liszkay, M. Maio, et al., Combined vemurafenib and cobimetinib in *BRAF*-mutated melanoma, N. Engl. J. Med. 371 (2014) 1867–1876.
[51] R. Dummer, P.A. Ascierto, H.J. Gogas, A. Arance, M. Mandala, G. Liszkay, et al., Encorafenib plus binimetinib versus vemurafenib or encorafenib in patients with

BRAF-mutant melanoma (COLUMBUS): a multicentre, open-label, randomised phase 3 trial, Lancet Oncol. 19 (2018) 603–615.
[52] K.S. Smalley, Z. Eroglu, V.K. Sondak, Combination therapies for melanoma: a new standard of care? Am. J. Clin. Dermatol. 17 (2016) 99–105.
[53] P. Sharma, J.P. Allison, The future of immune checkpoint therapy, Science 348 (2015) 56–61.
[54] J.J. Luke, K.T. Flaherty, A. Ribas, G.V. Long, Targeted agents and immunotherapies: optimizing outcomes in melanoma, Nat. Rev. Clin. Oncol. 14 (2017) 463–482.
[55] M. Kuske, D. Westphal, R. Wehner, M. Schmitz, S. Beissert, C. Praetorius, et al., Immunomodulatory effects of BRAF and MEK inhibitors: implications for melanoma therapy, Pharmacol. Res. 136 (2018) 151–159.
[56] M.C. Ramello, E.B. Haura, D. Abate-Daga, CAR-T cells and combination therapies: What's next in the immunotherapy revolution? Pharmacol. Res. 129 (2018) 194–203.
[57] A.M. Kidger, J. Sipthorp, S.J. Cook, ERK1/2 inhibitors: new weapons to inhibit the RAS-regulated RAF-MEK1/2-ERK1/2 pathway, Pharmacol. Ther. 187 (2018) 45–60.
[58] D.R. Knighton, J.H. Zheng, L.F. Ten Eyck, V.A. Ashford, N.H. Xuong, S.S. Taylor, J.M. Sowadski, Crystal structure of the catalytic subunit of cyclic adenosine monophosphate-dependent protein kinase, Science 253 (1991) 407–414.
[59] D.R. Knighton, J.H. Zheng, L.F. Ten Eyck, N.H. Xuong, S.S. Taylor, J.M. Sowadski, Structure of a peptide inhibitor bound to the catalytic subunit of cyclic adenosine monophosphate-dependent protein kinase, Science 253 (1991) 414–420.
[60] S.S. Taylor, A.P. Kornev, Protein kinases: evolution of dynamic regulatory proteins, Trends Biochem. Sci. 36 (2011) 65–77.
[61] A.P. Kornev, S.S. Taylor, Dynamics-driven allostery in protein kinases, Trends Biochem. Sci. 40 (2015) 628–647.
[62] R.S. Vijayan, P. He, V. Modi, K.C. Duong-Ly, H. Ma, J.R. Peterson, et al., Conformational analysis of the DFG-out kinase motif and biochemical profiling of structurally validated type II inhibitors, J. Med. Chem. 58 (2015) 466–479.
[63] A.J. Kooistra, A. Volkamer, Kinase-centric computational drug development, Ann. Rep. Med. Chem. 50 (2017) 197–236.
[64] R. Roskoski Jr, Cyclin-dependent protein serine/threonine kinase inhibitors as anticancer drugs, Pharmacol. Res. 139 (2019) 471–488.
[65] F. Zhang, A. Strand, D. Robbins, M.H. Cobb, E.J. Goldsmith, Atomic structure of the MAP kinase ERK2 at 2.3 Å resolution, Nature 367 (1994) 704–711.
[66] S.K. Hanks, T. Hunter, Protein kinases 6. The eukaryotic protein kinase superfamily: kinase (catalytic) domain structure and classification, FASEB J. 9 (1995) 576–596.
[67] C.S. Gibbs, M.J. Zoller, Rational scanning mutagenesis of a protein kinase identifies functional regions involved in catalysis and substrate interactions, J. Biol. Chem. 266 (1991) 8923–8931.
[68] Madhusudan, E.A. Trafny, N.H. Xuong, J.A. Adams, L.F. Ten Eyck, S.S. Taylor, J.M. Sowadski, cAMP-dependent protein kinase: crystallographic insights into substrate recognition and phosphotransfer, Protein Sci. 3 (1994) 176–187.
[69] J. Zhou, J.A. Adams, Participation of ADP dissociation in the rate-determining step in cAMP-dependent protein kinase, Biochemistry 36 (1997) 15733–15738.
[70] P.A. Schwartz, B.W. Murray, Protein kinase biochemistry and drug discovery, Bioorg. Chem. 39 (2011) 192–210.
[71] A.P. Kornev, S.S. Taylor, Defining the conserved internal architecture of a protein kinase, Biochim. Biophys. Acta 1804 (2010) 440–444.
[72] W.F. Waas, K.N. Dalby, Physiological concentrations of divalent magnesium ion activate the serine/threonine specific protein kinase ERK2, Biochemistry 42 (2003) 2960–2970.
[73] B.J. Canagarajah, A. Khokhlatchev, M.H. Cobb, E. Goldsmith, Activation mechanism of the MAP kinase ERK2 by dual phosphorylation, Cell 90 (1997) 859–869.
[74] R.J. Davis, The mitogen-activated protein kinase signal transduction pathway, J. Biol. Chem. 268 (1993) 14553–14556.
[75] D.A. Johnson, P. Akamine, E. Radzio-Andzelm, Madhusudan, S.S. Taylor, Dynamics of cAMP-dependent protein kinase, Chem. Rev. 101 (2001) 2243–2270.
[76] B.E. Kemp, D.J. Graves, E. Benjamini, E.G. Krebs, Role of multiple basic residues in determining the substrate specificity of cyclic AMP-dependent protein kinase, J. Biol. Chem. 252 (1977) 4888–4894.
[77] G. Pearson, F. Robinson, T. Beers Gibson, B.E. Xu, M. Karandikar, K. Berman, M.H. Cobb, Mitogen-activated protein (MAP) kinase pathways: regulation and physiological functions, Endocr. Rev. 22 (2001) 153–183.
[78] D. Jacobs, D. Glossip, H. Xing, A.J. Muslin, K. Kornfeld, Multiple docking sites on substrate proteins form a modular system that mediates recognition by ERK MAP kinase, Genes Dev. 13 (1999) 163–175.
[79] O. Bermudez, G. Pagès, C. Gimond, The dual-specificity MAP kinase phosphatases: critical roles in development and cancer, Am. J. Physiol., Cell Physiol. 299 (2010) C189–202.
[80] S.B. Hari, E.A. Merritt, D.J. Maly, Sequence determinants of a specific inactive protein kinase conformation, Chem. Biol. 20 (2013) 806–815.
[81] R. Roskoski Jr, A historical overview of protein kinases and their targeted small molecule inhibitors, Pharmacol. Res. 100 (2015) 1–23.
[82] A.P. Kornev, N.M. Haste, S.S. Taylor, L.F. Ten Eyck, Surface comparison of active and inactive protein kinases identifies a conserved activation mechanism, Proc. Natl. Acad. Sci. U. S. A. 103 (2006) 17783–17788.
[83] A.P. Kornev, S.S. Taylor, L.F. Ten Eyck, A helix scaffold for the assembly of active protein kinases, Proc. Natl. Acad. Sci. U. S. A. 105 (2008) 14377–14382.
[84] H.S. Meharena, P. Chang, M.M. Keshwani, K. Oruganty, A.K. Nene, N. Kannan, et al., Deciphering the structural basis of eukaryotic protein kinase regulation, PLoS Biol. 11 (2013) e1001690.
[85] R. Roskoski Jr, Classification of small molecule protein kinase inhibitors based upon the structures of their drug-enzyme complexes, Pharmacol. Res. 103 (2016) 26–48.
[86] R. Roskoski Jr, Anaplastic lymphoma kinase (ALK): structure, oncogenic activation, and pharmacological inhibition, Pharmacol. Res. 68 (2013) 68–94.
[87] R. Roskoski Jr, Anaplastic lymphoma kinase (ALK) inhibitors in the treatment of ALK-driven lung cancers, Pharmacol. Res. 117 (2017) 343–356.
[88] R. Roskoski Jr, Cyclin-dependent protein kinase inhibitors including palbociclib as anticancer drugs, Pharmacol. Res. 111 (2016) 784–803.
[89] R. Roskoski Jr, Cyclin-dependent protein serine/threonine inhibitors as anticancer drugs, Pharmacol. Res. 139 (2019) 471–488.
[90] R. Roskoski Jr, The ErbB/HER family of protein-tyrosine kinases and cancer, Pharmacol. Res. 79 (2014) 34–74.
[91] R. Roskoski Jr, ErbB/HER protein-tyrosine kinases: structures and small molecule inhibitors, Pharmacol. Res. 87 (2014) 42–59.
[92] R. Roskoski Jr, Small molecule inhibitors targeting the EGFR/ErbB family of protein-tyrosine kinases in human cancers, Pharmacol. Res. 139 (2019) 395–411.
[93] R. Roskoski Jr, Janus kinase (JAK) inhibitors in the treatment of inflammatory and neoplastic diseases, Pharmacol. Res. 111 (2016) 784–803.
[94] R. Roskoski Jr, The role of small molecule Kit protein-tyrosine kinase inhibitors in the treatment of neoplastic disorders, Pharmacol. Res. 133 (2018) 35–52.
[95] R. Roskoski Jr, The role of small molecule platelet-derived growth factor receptor (PDGFR) inhibitors in the treatment of neoplastic disorders, Pharmacol. Res. 129 (2018) 65–83.
[96] R. Roskoski Jr, A. Sadeghi-Nejad, Role of RET protein-tyrosine kinase inhibitors in the treatment RET-driven thyroid and lung cancers, Pharmacol. Res. 128 (2018) 1–17.
[97] R. Roskoski Jr, ROS1 protein-tyrosine kinase inhibitors in the treatment of ROS1 fusion protein-driven non-small cell lung cancers, Pharmacol. Res. 121 (2017) 202–212.
[98] R. Roskoski Jr, Src protein-tyrosine kinase structure, mechanism, and small molecule inhibitors, Pharmacol. Res. 94 (2015) 9–25.
[99] M.C. Frame, R. Roskoski Jr, Src family tyrosine kinases, Reference Module in Life Sciences, Elsevier, Amsterdam, 2017, pp. 1–11, https://doi.org/10.1016/B978-0-12-809633-8.07199-5.
[100] R. Roskoski Jr, Vascular endothelial growth factor (VEGF) and VEGF receptor inhibitors in the treatment of renal cell carcinomas, Pharmacol. Res. 120 (2017) 116–132.
[101] J. Kim, L.G. Ahuja, F.A. Chao, Y. Xia, C.L. McClendon, A.P. Kornev, et al., A dynamic hydrophobic core orchestrates allostery in protein kinases, Sci. Adv. 3 (2017) e1600663.
[102] Y. Liu, K. Shah, F. Yang, L. Witucki, K.M. Shokat, A molecular gate which controls unnatural ATP analogue recognition by the tyrosine kinase v-Src, Bioorg. Med. Chem. 6 (1998) 1219–1226.
[103] A.C. Dar, K.M. Shokat, The evolution of protein kinase inhibitors from antagonists to agonists of cellular signaling, Annu. Rev. Biochem. 80 (2011) 769–795.
[104] A. Vulpetti, R. Bosotti, Sequence and structural analysis of kinase ATP pocket residues, Farmaco 59 (2004) 759–765.
[105] T.A. Haystead, P. Dent, J. Wu, C.M. Haystead, T.W. Sturgill, Ordered phosphorylation of $p42^{mapk}$ by MAP kinase kinase, FEBS Lett. 306 (1992) 17–22.
[106] W.R. Burack, T.W. Sturgill, The activating dual phosphorylation of MAPK by MEK is nonprocessive, Biochemistry 36 (1997) 5929–5933.
[107] J.E. Ferrell, Jr, R.R. Bhatt, Mechanistic studies of the dual phosphorylation of mitogen-activated protein kinase, J. Biol. Chem. 272 (1997) 19008–19016.
[108] N.G. Anderson, J.L. Maller, N.K. Tonks, T.W. Sturgill, Requirement for integration of signals from two distinct phosphorylation pathways for activation of MAP kinase, Nature 343 (1990) 651–653.
[109] M.L. Hermiston, J. Zikherman, J.W. Zhu, CD45, CD148, and Lyp/Pep: critical phosphatases regulating Src family kinase signaling networks in immune cells, Immunol. Rev. 228 (2009) 288–311.
[110] P.J. Eichhorn, M.P. Creyghton, R. Bernards, Protein phosphatase 2A regulatory subunits and cancer, Biochim. Biophys. Acta 1795 (2009) 1–15.
[111] P.P. Ruvolo, Role of protein phosphatases in the cancer microenvironment, Biochim. Biophys. Acta Mol. Cell Res. 1866 (2019) 144–152.
[112] S.S. Taylor, M.M. Keshwani, J.M. Steichen, A.P. Kornev, Evolution of the eukaryotic protein kinases as dynamic molecular switches, Philos. Trans. R. Soc. Lond. Biol. Sci. 367 (2012) 2517–2528.
[113] F. Zuccotto, E. Ardini, E. Casale, M. Angiolini, Through the "gatekeeper door": exploiting the active kinase conformation, J. Med. Chem. 53 (2010) 2691–2694.
[114] L.K. Gavrin, E. Saiah, Approaches to discover non-ATP site inhibitors, Med. Chem. Res. 4 (2013) 41.
[115] V. Lamba, I. Ghosh, New directions in targeting protein kinases: focusing upon true allosteric and bivalent inhibitors, Curr. Pharm. Des. 18 (2012) 2936–2945.
[116] T.K. Johnson, M.B. Soellner, Bivalent inhibitors of c-Src tyrosine kinase that bind a regulatory domain, Bioconjug. Chem. 27 (2016) 1745–1749.
[117] F.E. Kwarcinski, K.R. Brandvold, S. Phadke, O.M. Beleh, T.K. Johnson, J.L. Meagher, et al., Conformation-selective analogues of dasatinib reveal insight into kinase inhibitor binding and selectivity, ACS Chem. Biol. 11 (2016) 1296–1304.
[118] Z. Zhao, H. Wu, L. Wang, Y. Liu, S. Knapp, Q. Liu, N.S. Gray, Exploration of type II binding mode: A privileged approach for kinase inhibitor focused drug discovery? ACS Chem. Biol. 9 (2014) 1230–1241.
[119] R.A. Copeland, The drug-target residence time model: a 10-year retrospective, Nat. Rev. Drug Discov. 15 (2016) 87–95.
[120] P.M. Ung, R. Rahman, A. Schlessinger, Redefining the protein kinase conformational space with machine learning, Cell Chem. Biol. 25 (2018) 916-24.e2.

[121] J.J. Liao, Molecular recognition of protein kinase binding pockets for design of potent and selective kinase inhibitors, J. Med. Chem. 50 (2007) 409–424.
[122] O.P. van Linden, A.J. Kooistra, R. Leurs, I.J. de Esch, C. de Graaf, KLIFS: a knowledge-based structural database to navigate kinase-ligand interaction space, J. Med. Chem. 57 (2014) 249–277.
[123] D. Bajusz, G.G. Ferenczy, G.M. Keserá, Structure-based virtual screening approaches in kinase-directed drug discovery, Curr. Top. Med. Chem. 17 (2017) 2235–2259.
[124] D. Fabbro, S.W. Cowan-Jacob, H. Moebitz, Ten things you should know about protein kinases: IUPHAR Review 14, Br. J. Pharmacol. 172 (2015) 2675–2700.
[125] G. Cavallo, P. Metrangolo, R. Milani, T. Pilati, A. Priimagi, G. Resnati, et al., The halogen bond, Chem. Rev. 116 (2016) 2478–2601.
[126] F. Carles, S. Bourg, C. Meyer, P. Bonnet, PKIDB: a curated, annotated and updated database of protein kinase inhibitors in clinical trials, Molecules 23 (2018), https://doi.org/10.3390/molecules23040908.
[127] U.A. Germann, B.F. Furey, W. Markland, R.R. Hoover, A.M. Aronov, J.J. Roix, et al., Targeting the MAPK signaling pathway in cancer: promising preclinical activity with the novel selective ERK1/2 inhibitor BVD-523 (ulixertinib), Mol. Cancer Ther. 16 (2017) 2351–2363.
[128] R.J. Sullivan, J.R. Infante, F. Janku, D.J.L. Wong, J.A. Sosman, V. Keedy, et al., First-in-class ERK1/2 inhibitor ulixertinib (BVD-523) in patients with MAPK mutant advanced solid tumors: results of a phase I dose-escalation and expansion study, Cancer Discov. 8 (2018) 184–195.
[129] S.B. Boga, Y. Deng, L. Zhu, Y. Nan, A.B. Cooper, G.W. Shipps Jr, R. Doll, et al., MK-8353: discovery of an orally bioavailable dual mechanism ERK inhibitor for oncology, ACS Med. Chem. Lett. 9 (2018) 761–767.
[130] S.J. Moschos, R.J. Sullivan, W.J. Hwu, R.K. Ramanathan, A.A. Adjei, P.C. Fong, et al., Development of MK-8353, an orally administered ERK1/2 inhibitor, in patients with advanced solid tumors, JCI Insight 3 (2018) pii:92352.
[131] J.F. Blake, M. Burkard, J. Chan, H. Chen, K.J. Chou, D. Diaz, et al., Discovery of (*S*)-1-(1-(4-Chloro-3-fluorophenyl)-2-hydroxyethyl)-4-(2-((1-methyl-1*H*-pyrazol-5-yl)amino)pyrimidin-4-yl)pyridin-2(1*H*)-one (GDC-0994), an extracellular signal-regulated kinase 1/2 (ERK1/2) inhibitor in early clinical development, J. Med. Chem. 59 (2016) 5650–5660.
[132] E.J. Morris, S. Jha, C.R. Restaino, P. Dayananth, H. Zhu, A. Cooper, et al., Discovery of a novel ERK inhibitor with activity in models of acquired resistance to BRAF and MEK inhibitors, Cancer Discov. 3 (2013) 742–750.
[133] T.D. Heightman, V. Berdini, H. Braithwaite, I.M. Buck, M. Cassidy, J. Castro, et al., Fragment-based discovery of a potent, orally bioavailable inhibitor that modulates the phosphorylation and catalytic activity of ERK1/2, J. Med. Chem. 61 (2018) 4978–4992.
[134] M. Wang, L. Zhang, Z. Liu, J. Zhou, Q. Pan, J. Fan, et al., AGO1 may influence the prognosis of hepatocellular carcinoma through TGF-β pathway, Cell Death Dis. 9 (2018) 324.
[135] I. Aronchik, Y. Dai, M. Labenski, C. Barnes, T. Jones, L. QIao, L. Beebe, et al., Efficacy of a covalent ERK1/2 inhibitor, CC-90003, in KRAS mutant cancer models reveals novel mechanisms of response and resistance, Mol. Cancer Res. (2018) pii: molcanres.0554.2017.
[136] F. Liu, X. Yang, M. Geng, M. Huang, Targeting ERK, an Achilles' heel of the MAPK pathway, in cancer therapy, Acta Pharm. Sin. B 8 (2018) 552–562.
[137] B.S. Jaiswal, S. Durinck, E.W. Stawiski, J. Yin, W. Wang, E. Lin, et al., ERK mutations and amplification confer resistance to ERK-inhibitor therapy, Clin. Cancer Res. 24 (2018) 4044–4055.
[138] C.A. Lipinski, F. Lombardo, B.W. Dominy, P.J. Feeney, Experimental and computational approaches to estimate solubility and permeability in drug discovery and development settings, Adv. Drug Deliv. Rev. 23 (1997) 3–25.
[139] A.L. Hopkins, C.R. Groom, A. Alex, Ligand efficiency: a useful metric for lead selection, Drug Discov. Today 9 (2004) 430–431.
[140] G.F. Smith, Medicinal chemistry by the numbers: the physicochemistry, thermodynamics and kinetics of modern drug design, Prog. Med. Chem. 48 (2009) 1–29.
[141] P.D. Leeson, B. Springthorpe, The influence of drug-like concepts on decision-making in medicinal chemistry, Nat. Rev. Drug Discov. 6 (2007) 881–890.
[142] C.A. Lipinski, Rule of five in 2015 and beyond: target and ligand structural limitations, ligand chemistry structure and drug discovery project decisions, Adv. Drug Deliv. Rev. 101 (2016) 34–41.
[143] S. Ekins, N.K. Litterman, C.A. Lipinski, B.A. Bunin, Thermodynamic proxies to compensate for biases in drug discovery methods, Pharm. Res. 33 (2016) 194–205.
[144] A.L. Hopkins, G.M. Keserü, P.D. Leeson, D.C. Rees, C.H. Reynolds, The role of ligand efficiency metrics in drug discovery, Nat. Rev. Drug Discov. 13 (2014) 105–121.
[145] P.D. Leeson, Molecular inflation, attrition, and the rule of five, Adv. Drug Deliv. Rev. 101 (2016) 22–33.
[146] M.M. Cavalluzzi, G.F. Mangiatordi, O. Nicolotti, G. Lentini, Ligand efficiency metrics in drug discovery: the pros and cons from a practical perspective, Expert Opin. Drug Discov. 12 (2017) 1087–1104.
[147] S.H. Myers, V.G. Brunton, A. Unciti-Broceta, AXL inhibitors in cancer: a medicinal chemistry perspective, J. Med. Chem. 59 (2016) 3593–3608.
[148] B.L. Roth, D.J. Sheffler, W.K. Kroeze, Magic shotguns versus magic bullets: selectively non-selective drugs for mood disorders and schizophrenia, Nat. Rev. Drug Discov. 3 (2004) 353–359.
[149] P.L. Kaufman, M.E. Mohr, S.P. Riccomini, C.A. Rasmussen, Glaucoma drugs in the pipeline, Asia Pac. J. Ophthalmol. (Phila.) 7 (2018) 345–351.
[150] P. Cohen, D.R. Alessi, Kinase drug discovery–what's next in the field? ACS Chem. Biol. 8 (2013) 96–104.
[151] K. Budzyn, P.D. Marley, C.G. Sobey, Targeting Rho and Rho-kinase in the treatment of cardiovascular disease, Trends Pharmacol. Sci. 27 (2006) 97–104.
[152] D.M. Goldstein, A. Kuglstatter, Y. Lou, M.J. Soth, Selective p38α inhibitors clinically evaluated for the treatment of chronic inflammatory disorders, J. Med. Chem. 53 (2010) 2345–2353.
[153] C.C. Mok, The jakinibs in systemic lupus erythematosus: progress and prospects, Expert Opin. Investig. Drugs 28 (2019) 85–92.
[154] H. Schenck Eidam, J. Russell, K. Raha, M. DeMartino, D. Qin, H.A. Guan, et al., Discovery of a first-in-class gut-restricted RET kinase inhibitor as a clinical candidate for the treatment of IBS, ACS Med. Chem. Lett. 9 (2018) 623–628.
[155] S. Wan, A.P. Bhati, S. Skerratt, K. Omoto, V. Shanmugasundaram, S.K. Bagal, et al., Evaluation and characterization of Trk kinase inhibitors for the treatment of pain: reliable binding affinity predictions from theory and computation, J. Chem. Inf. Model. 57 (2017) 897–909.
[156] M. Golpich, E. Amini, F. Hemmati, N.M. Ibrahim, B. Rahmani, Z. Mohamed, et al., Glycogen synthase kinase-3 beta (GSK-3β) signaling: implications for Parkinson's disease, Pharmacol. Res. 97 (2015) 16–26.
[157] V. Nozal, A. Martinez, Tau Tubulin Kinase 1 (TTBK1), a new player in the fight against neurodegenerative diseases, Eur. J. Med. Chem. 161 (2019) 39–47.
[158] H.B. Nygaard, A.F. Wagner, G.S. Bowen, S.P. Good, M.G. MacAvoy, K.A. Strittmatter, et al., A phase Ib multiple ascending dose study of the safety, tolerability, and central nervous system availability of AZD0530 (saracatinib) in Alzheimer's disease, Alzheimers Res. Ther. 7 (2015) 35.
[159] M. Siu, A. Sengupta Ghosh, J.W. Lewcock, Dual leucine zipper kinase inhibitors for the treatment of neurodegeneration, J. Med. Chem. 61 (2018) 8078–8087.
[160] V. Palomo, D.I. Perez, C. Roca, C. Anderson, N. Rodríguez-Muela, C. Perez, et al., Subtly modulating glycogen synthase kinase 3 β: allosteric inhibitor development and their potential for the treatment of chronic diseases, J. Med. Chem. 60 (2017) 4983–5001.
[161] F.M. Ferguson, N.S. Gray, Kinase inhibitors: the road ahead, Nat. Rev. Drug Discov. 17 (2018) 353–377.
[162] A.M. Joussen, S. Wolf, P.K. Kaiser, D. Boyer, T. Schmelter, R. Sandbrink, et al., The Developing regorafenib eye drops for neovascular age-related macular degeneration (DREAM) study: an open-label phase II trial, Br. J. Clin. Pharmacol. (2018), https://doi.org/10.1111/bcp.13794.
[163] R. Nussinov, H. Jang, C.J. Tsai, F. Cheng, Precision medicine review: rare driver mutations and their biophysical classification, Biophys. Rev. (2019), https://doi.org/10.1007/s12551-018-0496-2.
[164] H.G. Williams-Ashman, E.P. Kennedy, Oxidative phosphorylation catalyzed by cytoplasmic particles isolated from malignant tissues, Cancer Res. 12 (1952) 415–421.
[165] E.P. Kennedy, S.W. Smith, The isolation of radioactive phosphoserine from phosphoprotein of the Ehrlich ascites tumor, J. Biol. Chem. 207 (1954) 153–163.
[166] G. Burnett, E.P. Kennedy, The enzymatic phosphorylation of proteins, J. Biol. Chem. 211 (1954) 969–980.
[167] L. Tao, F. Zhu, F. Xu, Z. Chen, Y.Y. Jiang, Y.Z. Chen, Co-targeting cancer drug escape pathways confers clinical advantage for multi-target anticancer drugs, Pharmacol. Res. 102 (2015) 123–131.
[168] R. Roskoski Jr, Guidelines for preparing color figures for everyone including the colorblind, Pharmacol. Res. 119 (2017) 240–241 Erratum in: Pharmacol Res. 139, 2019, 569. pii: S1043-6618(18)31424-5. doi: 10.1016/j.phrs.2018.09.019.